

CHEMOMETRIC METHOD TO ENHANCE SENSITIVITY AND SELECTIVITY FOR SURFACE
ENHANCED RAMAN SCATTERING TECHNIQUE



A Thesis Submitted in Partial Fulfillment of the Requirements
for the Degree of Master of Science in Chemistry
Department of Chemistry
FACULTY OF SCIENCE
Chulalongkorn University
Academic Year 2019
Copyright of Chulalongkorn University

ระเบียบวิธีทางเคมีเมทริกซ์เพื่อเพิ่มสภาพไวและการเลือกจำเพาะสำหรับเทคนิคเซอร์เฟซเอ็นฮานซ์
นซ์รามานสแกตเทอริง



วิทยานิพนธ์นี้เป็นส่วนหนึ่งของการศึกษาตามหลักสูตรปริญญาวิทยาศาสตรมหาบัณฑิต
สาขาวิชาเคมี ภาควิชาเคมี
คณะวิทยาศาสตร์ จุฬาลงกรณ์มหาวิทยาลัย
ปีการศึกษา 2562
ลิขสิทธิ์ของจุฬาลงกรณ์มหาวิทยาลัย

Thesis Title	CHEMOMETRIC METHOD TO ENHANCE SENSITIVITY AND SELECTIVITY FOR SURFACE ENHANCED RAMAN SCATTERING TECHNIQUE
By	Mr. Nontawat Sricharoen
Field of Study	Chemistry
Thesis Advisor	Associate Professor KANET WONGRAVEE, Ph.D.
Thesis Co Advisor	Assistant Professor PROMPONG PIENPINIJTHAM, Ph.D.

Accepted by the FACULTY OF SCIENCE, Chulalongkorn University in Partial Fulfillment
of the Requirement for the Master of Science

..... Dean of the FACULTY OF SCIENCE
()

THESIS COMMITTEE

..... Chairman
(Associate Professor VUDHICHAJ PARASUK, Ph.D.)
..... Thesis Advisor
(Associate Professor KANET WONGRAVEE, Ph.D.)
..... Thesis Co-Advisor
(Assistant Professor PROMPONG PIENPINIJTHAM, Ph.D.)
..... Examiner
(Associate Professor VIWAT VCHIRAWONGKWIN, Dr.rer.nat.)
..... External Examiner
(Suwussa Bamrungsap, Ph.D.)

นลธวัช ศรีเจริญ : ระเบียบวิธีทางเคมีเมทริกซ์เพื่อเพิ่มสภาพไวและการเลือกจำเพาะสำหรับเทคนิค เซอร์เฟซเอ็นฮานซ์รามานสแกตเทอริง. (CHEMOMETRIC METHOD TO ENHANCE SENSITIVITY AND SELECTIVITY FOR SURFACE ENHANCED RAMAN SCATTERING TECHNIQUE) อ.ที่
 ปรึกษาหลัก : รศ. ดร.คณิศ วังษ์ระวี, อ.ที่ปรึกษาร่วม : ผศ. ดร.พร้อมพงศ์ เพียรพิณจรธรรม

อัลกอริทึมการแยกชุดข้อมูลหลายตัวแปร-สมการการถดถอยกำลังสองทางเลือก (MCR-ALS) ได้ถูกดัดแปลงด้วยข้อจำกัดการเพิ่มจำนวนตัวอย่าง การพัฒนานี้ได้เสนอเพื่อที่จะใช้ในการแก้ไขการทับซ้อนกันของข้อมูลที่ได้จากสัญญาณจากเทคนิคเซอร์เฟซเอ็นฮานซ์รามานสแกตเทอริง (Surface-enhanced Raman scattering, SERS) โดยโปรแกรมพัฒนาขึ้นถูกทดสอบด้วยสเปกตรัมที่สังเคราะห์ขึ้นมาโดยอาศัยสมการการกระจายแบบเกาส์เซียน สเปกตรัมที่สังเคราะห์ขึ้นจะประกอบด้วยสัญญาณสองพีคที่ไม่มีเกี่ยวข้องกัน โดยพีคหนึ่งเป็นของสารปรับปรุงพื้นผิว (vapping agent) และอีกพีคหนึ่งเป็นสัญญาณของสารเป้าหมาย (analyte) สัญญาณทั้งสองนี้จะถูกสังเคราะห์ขึ้นโดยมีการซ้อนทับกันในช่วง $0 - 1.5$ ($RS = 0 - 1.5$) และสัดส่วนความเข้มข้นของสารเป้าหมายต่อสารปรับปรุงพื้นผิวมีค่าในช่วง $0.01 - 1.00$ ในวิเคราะห์ข้อมูลด้วยเทคนิค MCR-ALS นั้นจะทำการเพิ่มจำนวนข้อมูลของสารปรับปรุงพื้นผิวอยู่ในช่วง $10 - 100$ เท่า จากการวิเคราะห์สเปกตรัมสังเคราะห์ด้วยเทคนิค MCR-ALS ที่พัฒนาขึ้น พบว่าหลังจากการแยกสัญญาณของสารปรับปรุงพื้นผิวออกแบบจำลองมาตรฐาน (calibration model) ของสารเป้าหมายถูกสร้างขึ้น ด้วยค่าความถูกต้องที่ $R^2 > 0.92$ ในทุกภาวะ และจำนวนข้อมูลของสารปรับปรุงพื้นผิวที่เพิ่มนั้นได้ถูกออกแบบให้มีการคำนวณแบบอัตโนมัติ จากนั้นวิธีการ MCR-ALS ที่พัฒนาขึ้นนั้น ได้ถูกนำไปประยุกต์ใช้กับข้อมูลจากการทดลองจริง ที่เป็นการตรวจวัดสัญญาณ SERS เพื่อหาปริมาณของคาร์โบฟูแรน (carbofuran) โดยปฏิกิริยาคู่ควบเอโซ (azo-coupling reaction) กับพารา-อะมิโนไทโอฟีนอลบนอนุภาคระดับนาโนเมตรของเงิน ที่ใช้เป็นตัวเร่งสัญญาณรามาน จากผลการวิเคราะห์นั้นสามารถให้แบบจำลองมาตรฐานไปวิเคราะห์ความเข้มข้นคาร์โบฟูแรนจากชุดทดสอบ (validation set) พบว่าค่ารากที่สองของค่าเฉลี่ยความคลาดเคลื่อนจากการทำนาย ($RMSE$) = 2.109 และ $R^2 = 0.97$

สาขาวิชา เคมี
 ปีการศึกษา 2562

ลายมือชื่อนิสิต
 ลายมือชื่อ อ.ที่ปรึกษาหลัก
 ลายมือชื่อ อ.ที่ปรึกษาร่วม

6072067623 : MAJOR CHEMISTRY

KEYWORD: MCR-ALS, SERS, sample insertion, Chemometric method, spectroscopy

Nontawat Sricharoen : CHEMOMETRIC METHOD TO ENHANCE SENSITIVITY AND SELECTIVITY FOR SURFACE ENHANCED RAMAN SCATTERING TECHNIQUE. Advisor: Assoc. Prof. KANET WONGRAVEE, Ph.D. Co-advisor: Asst. Prof. PROMPONG PIENPINIJTHAM, Ph.D.

The multivariate curve resolution-alternative least square (MCR-ALS) algorithm was modified with sample insertion constraint. This developed method was proposedly used to deconvolute the overlapping signals in Surface enhance Raman attering (SERS) measurement. The developed method was elucidated with the spectral data simulated by using Gaussian distribution function to generate two independent peaks which correspond to capping agent and analyte, respectively. The spectrum of the two peaks was generated with different overlapping levels ($RS = 0 - 1.50$) and concentration ratio of analyte and capping agent concentration at $0.01 - 1.00$. In MCR-ALS with sample insertion constraint, the number of capping agent spectra were added in the range of $10 - 100$ times. After excluding the signal from the capping agent, the calibration model of the analyte was built with $R^2 > 0.92$ in all conditions. The obtained calibration model is dramatically improved compared with the model generated using either conventional background subtraction or original MCR-ALS. In the case, the appropriate number of added spectra was automatically optimized. Furthermore, our developed method was performed on a real SERS measurement to quantify carbofuran (analyte) by using azo-coupling reaction with *p*-ATP (capping agent) on the silver nanoparticles as SERS substrate. The calibration model was generated with R^2 values = 0.99 and LOD = 28.19 ppm which highly improved with the conventional methods. To access the performance of the calibration model, the model was used to estimate the concentrations of carbofuran in an external validation set. It was found that root mean square error (*RMSE*) of prediction was only 2.109 and $R^2 = 0.97$.

Field of Study: Chemistry

Student's Signature

Academic Year: 2019

Advisor's Signature

Co-advisor's Signature

ACKNOWLEDGEMENTS

Firstly, I would like to express my gratitude to my thesis advisor Associate Professor Dr. Kanet Wongravee. This thesis cannot be successfully done without the help of my thesis advisor who gives the great guidance, generous training, and considerate understanding. I would also like to express my gratitude to my co-advisor Assistance Professor Dr. Prompong Pienpinijtham, Professor Dr. Sanong Ekgasit for kind suggestion and detailed direction in the scientific knowledge and laboratory skill. And I would like to thanks all of my colleagues, Sensor Research Unit (SRU) member, for all hospitality, help and support during my time doing the thesis.

Finally, this thesis was supported in the financial from Center of Excellence on Petrochemical and Materials Tecchnology (PETROMAT), Department of Chemistry, Faculty of Science Chulalongkorn University for hospitable supporting and powerful encouragement throughout the research.

Nontawat Sricharoen



TABLE OF CONTENTS

	Page
.....	iii
ABSTRACT (THAI)	iii
.....	iv
ABSTRACT (ENGLISH)	iv
ACKNOWLEDGEMENTS	v
TABLE OF CONTENTS	vi
LIST OF TABLES	viii
LIST OF FIGURES	ix
LIST OF ABBREVIATIONS	xii
CHAPTER I INTRODUCTION	1
1.1 Problem and background	1
1.2 Objective	7
1.3 Scope of this work	8
CHAPTER II THEORITICAL BACKGROUND	9
2.1 Raman Spectroscopy	9
2.2 Localized surface plasmon resonance (LSPR)	10
2.3 Surface-enhanced Raman scattering (SERS)	11
2.4 Multivariate Curve Resolution-Alternative Least Square (MCR-ALS)	12
CHAPTER III EXPERIMENTAL SECTION	16
3.1 Spectrum simulation	16
3.2 Removal of Main components in SERS signal	19
3.3 Performance Indices	22
3.4 Real system (quantify carbofuran using SERS)	23
CHAPTER IV RESULTS AND DISCUSSION	25
4.1 Spectral simulation	25
4.2 Real system (quantify carbofuran using SERS)	32

CHAPTER V CONCLUSION.....	37
APPENDIX.....	38
REFERENCES	40
VITA.....	45



LIST OF TABLES

Table 1.1 Literature reviews of determination of SERS technique combined with chemometric methods	5
Table 4.1 SERS peak assignment for <i>p</i> -mercaptophenol and carbofuran-derived azo compound.....	33



LIST OF FIGURES

Figure 1.1 Problematic observation in SERS measurement in order to quantify amount of target analyte when excessive amount of capping agent is used and the overlapped SERS signals between the capping agent and the target analyte are occurred.	2
Figure 1.2 Schematic of the MCR-ALS techniques.....	3
Figure 2.1 Energy level diagram involving Rayleigh scattering and Raman scattering.....	9
Figure 2.2 Localized surface plasmon resonance (LSPR).....	11
Figure 2.3 Illustration of a hot spot generated between the gap of the nanoparticles. The SERS enhancement related with the gap size of the connected nanoparticles	12
Figure 2.4 Scheme of the step of MCR-ALS GUI that was used in this work.....	15
Figure 3.1 (A) pure spectra of analyte (s_{ana}) at the different RS values compared with pure spectra of capping agent (s_{cap}) (blue line) when the red, green, cyan, purple, and yellow line represent the s_{ana} at $RS = 1.5, 0.8, 0.5, 0.2,$ and $0,$ respectively. (B1) – (B5) the combined of s_{ana} and s_{cap} at the RS values = $1.5, 0.8, 0.5, 0.2,$ and $0,$ respectively. The decrease of the RS values the peak the analyte moved closer to the peak of the capping agent and more overlapped. ANA and CAP are represent analyte and capping agent, respectively.....	17
Figure 3.2 The simulated spectra from A) – E) the ratio of the concentration of the analyte were varied form $0.01-0.20, 0.21-0.40, 0.41-0.60, 0.61-0.80,$ and $0.81-1.00$ and 1) - 5) the RS values were varied from $1.5, 0.8, 0.5, 0.2,$ and $0,$ respectively. The red, blue and grey line represent the highest, lowest and moderate concentration of the analyte. ANA and CAP represent the analyte and capping agent peaks, respectively.	18
Figure 3.3 Scheme describe the extraction of capping agent signal by using sample insertion constraint with MCR-ALS method and Remove the signal of	

- capping agent and construct the standard calibration curve from the analyte signal which then is used to predict the test samples21
- Figure 3.4 SERS measurement of carbofuran via diazo-coupling reaction with *p*-ATP when AgNPs colloid is used as SERS substrate24
- Figure 4.1(A) The contour map of R^2 value of the calibration curve calculated from analyte peak extracted by criterion (I) background subtraction, (II) MCR-ALS and (III) MCR-ALS with sample insertion constrain. (B) the calibration curve plot from point (I), (II), (III), (IV), and (V) on the contour map with the inset Figures as the analyte peak after extraction. All Figures are in the same scale of intensity and concentration (a.u.)27
- Figure 4.2 (A1) The contour map of the sample ratio appropriately added to the data matrix to completely removed the capping agent peak. The map of mean absolute percentage error (*MAPE*) of calibration set (A2) and validation set (A3) at different conditions. (B1-B3) Plot of the MCR-ALS predicted concentrations versus actual concentrations using the sample insertion constraint for $RS = 0, 0.2$ and 0.5 respectively. Inset Figures of B1-B3 demonstrate the original simulated spectra of calibration set (black), the simulated spectra for validation set (grey), the extracted spectra of calibration set (blue) and the extracted spectra of validation set (red).29
- Figure 4.3 (A) The Euclidean distance of the preset spectra and the extracted spectra of capping agent at the various number of the added capping agent. The black square, red circle, blue triangle, green triangle, and purple diamond are the distance at the different concentration ratios from 0.01-0.20, 0.21-0.40, 0.41-0.60, 0.61-0.80, and 0.81-1.00, respectively. (B) the preset spectra (black line) and the extracted spectra of the capping agent using sample insertion at 10 (red dash line), 40 (blue dash line) and 100 (green dash line) times, respectively. The inset Figures show the spectra at the 1700 cm^{-1} with condition of $RS = 0.5$31
- Figure 4.4 SERS spectra of azo compounds derived from carbofuran of 0.1-100 ppm. The yellow highlight is the region that was used to examine the

relationship between the intensity and concentration. The yellow highlight is the selected peaks to find the relation between intensity and concentration.....	33
Figure 4.5 The R^2 values by varied the Ratio of added capping agent at 5, 10, 50, 100, and 150 times	34
Figure 4.6 (A) SERS spectra of azo compounds at peak 1570 cm^{-1} and the calibration curve with $R^2 = 0.731$. (B) SERS spectra after MCR-ALS extraction with sample insertion constraint and the calibration curve with $R^2 = 0.990$. The yellow highlight is the selected peaks to find the relation between intensity and concentration	35
Figure 4.7 Predicted concentration versus presetting concentration in the carbofuran derived azo-compound at the 1570 cm^{-1} peaks the black square and red circle represent the calibration and validation set, respectively by the $RMSEC$ is the $RMSE$ values of calibration and $RMSEP$ is the $RMSE$ of the validation sets.....	36
Figure 1 The calibration curve plot from analyte peak extracted by criterion (I) background subtraction, (II) MCR-ALS and (III) MCR-ALS with sample insertion constrain on the $RS = 0$ at the various concentration ratio of the analyte	38
Figure 2 The calibration curve plot from analyte peak extracted by criterion (I) background subtraction, (II) MCR-ALS and (III) MCR-ALS with sample insertion constrain on the $RS = 0.2$ at the various concentration ratio of the analyte	39

LIST OF ABBREVIATIONS

A	Peak intensity
α	Concentration ratio
a	Coefficient
C	Concentration profiles
\hat{C}	Estimated concentration profiles
C_{cap}	Concentration profiles matrix of the capping agent
C_{ana}	Concentration profiles matrix of the analyte
$Conc$	Concentration
c	Point of the concentration profile
c_1	Concentration of the first component
c_2	Concentration profiles of the second component
c_{cap}	Concentration profiles of the capping agent
c_{ana}	Concentration profiles of the analyte
E	Error or variance matrix
e	Noise of the data matrix
h	Planck constant
m	Mean
σ	Standard deviation
p	Peak position
R^2	Correlation coefficient
RS	Resolution
S	Pure spectra profiles
\hat{S}	Estimated pure spectra
S_{cap}	Pure spectra matrix of the capping agent
S_{ana}	Pure spectra matrix of the analyte
s	Point of the pure spectra profiles

s_1	Spectral profiles of the first component
s_2	Spectral profiles of the second component
s_{cap}	Pure spectra of the capping agent
s_{ana}	Pure spectra of the analyte
μ	Peak position
ν	Spectral variables
ω	Frequency
w	Width of peak
X	Data matrix (spectra)
\hat{X}	Estimated data
X_{ana}	Analyte spectra
X_{cap}	Capping agent spectra
x	Data point of the spectra
Y	Response
AgNPs	Silver nanoparticles
AgNO ₃	Silver nitrate
AuNPs	Gold nanoparticles
HCl	Hydrochloric
KOH	Potassium hydroxide
Na ₃ C ₆ H ₅ O ₇	Tri-sodium citrate
NaNO ₂	Sodium nitrate
<i>p</i> -ATP	<i>Para</i> -aminothiophenol
<i>ARPE</i>	Average relative prediction error
CARS-BP-AsaBoost	Competitive-adaptive reweighted sampling BP- AdaBoost
GA-PLS	Genetic algorithm-partial least squares
LOD	Limit of detection

LOQ	Limit of quantitation
<i>MAPE</i>	Mean average percent error
MEM_{SERS}	Multiplicative effect model for surface-enhanced Raman spectroscopy
PCA	Principal component analysis
PLSR	Partial Least Square regression
<i>RMSEC</i>	Root mean square error of calibration
<i>RMSEP</i>	Root mean square error of prediction
ANA	Analyte spectra
CAP	Capping agent spectra
IR	Infrared
LSPR	Localized surface plasmon resonance
MCR-ALS	Multivariate Curve Resolution-Alternative Least Square
MNPs	Metal nanoparticles
mW	Milliwatts
NPs	Nanoparticles
nm	Nanometers
<i>nls</i>	Non-negative least square
<i>RMSE</i>	Root mean square errors
SERS	Surface-Enhanced Raman Scattering
SP	Surface plasmon
μm	Micrometers

CHAPTER I

INTRODUCTION

1.1 Problem and background

Surface-enhanced Raman scattering (SERS) spectroscopy is a rapid and ultrasensitive technique for detecting the vibrational signatures of target molecules. This technique has dramatically gained considerable attention in recent years due to its versatility and high selectivity and sensitivity¹⁻⁴. To enhance Raman scattering efficiency, a target molecule should diffuse close proximity to a surface of metallic nanostructures such as Ag, Au or Pt.⁵⁻¹⁰ The appropriate types of metal should complementally depend on the frequency of a laser light source in order to generate strong local electromagnetic near-field.¹¹⁻¹⁴ Although SERS has the potential to be used as a general sensing platform, but its poor selectivity is an important limitation for quantifying the target analytes in the complex matrices.

To overcome the limitation, an integration step with separation of the sample was employed to circumvent this issue. However, this additional separation step involves complicated route, time-consuming and some of analytes might be lost during the process¹⁵⁻¹⁷. Therefore, functionalization of the nano-surface with selective and specific capping agents has been preferred and successfully employed to deal with the limitation^{14, 18-21}. The capping agent should be designed to contain functional groups which easily interact with the target analyte. Due to the interaction, the signal patterns between the capping agents and the target analyte can be either partially or completely overlapped. From SERS measurement, the combination signals of the capping agent and the target analyte were obviously occurred. Therefore, the functional groups of capping agents and the analyte must be carefully considered and chosen. In the case, if the affinity and absorptivity of the analyte to the metal surface is abundant to overcome the signal generated from the capping agents, its quantification might be performed even presenting overlapping bands by curve fitting and some multivariate data analysis methods^{19, 22-25} However, amount of the capping agent is particularly excessively added to fully cover an extensive surface of SERS substrate (metal surface) and the analyte is usually in trace amount as shown in Figure 1.1. Therefore, to quantify the signal selectively to the target analyte might be

complicated and difficult. It is not possible to obtain only analyte information by either directly measuring of peak intensity or using conventional background subtraction^{22, 24}.

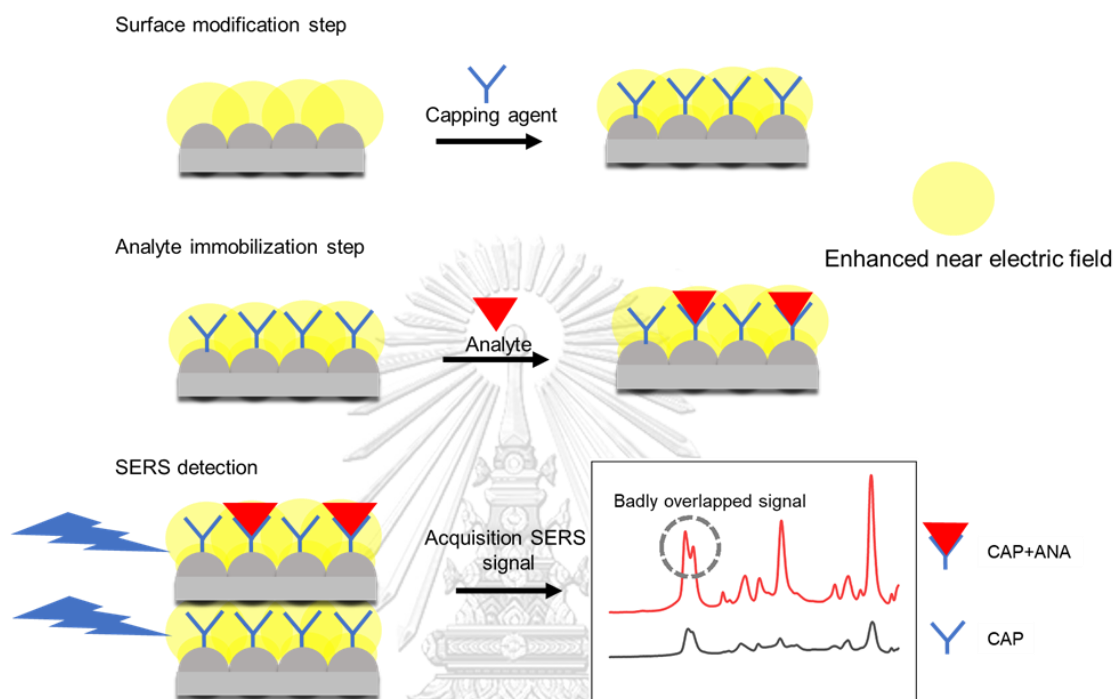


Figure 1.1 Problematic observation in SERS measurement in order to quantify amount of target analyte when excessive amount of capping agent is used and the overlapped SERS signals between the capping agent and the target analyte are occurred

CHULALONGKORN UNIVERSITY

To solve the problem stated above, chemometrics provides the great advantage to discover and extract analytical information from a complex mixture using the statistical and mathematical approaches. Conventional linear analysis such as Multiple Linear Regression (MLR)²⁶⁻²⁹ and Principal Component Regression (PCR)²⁶⁻³² are commonly employed to interpret the relationships between the independent variables (Raman spectra in the case) and dependent variable (the analyte concentration)³³⁻³⁹.

Although they are easy to program, simple and provide good predictive performance but they do not properly handle any collinearity presented in the data and they risks to overfit problems^{23, 40}. Therefore, Partial Least Square regression (PLSR) is probably the most popular multivariate calibration techniques employed in quantitative analysis^{23, 41-44}. The golden aim of PLSR is to establish a calibration model of multivariate data to predict the analyte concentrations even in the presence of interferences. Thus, PLSR usually provides high predictive accuracy for spectroscopic data but it lacks of the capability to reveal any qualitative information about the analytes e.g. vibrational modes of functional groups and spectral pattern of the target molecule. Moreover, from analytical point of view, the standard performance indices such as the limit of detection (LOD) and limit of quantitation (LOQ) of the multivariate calibration model are difficult to be defined by PLSR⁴⁵. To prevent the problems, Multivariate curve resolution-alternative least square (MCR-ALS) can better overcome the problems and provide significant advantages relative to univariate analyses^{23, 46-51}.

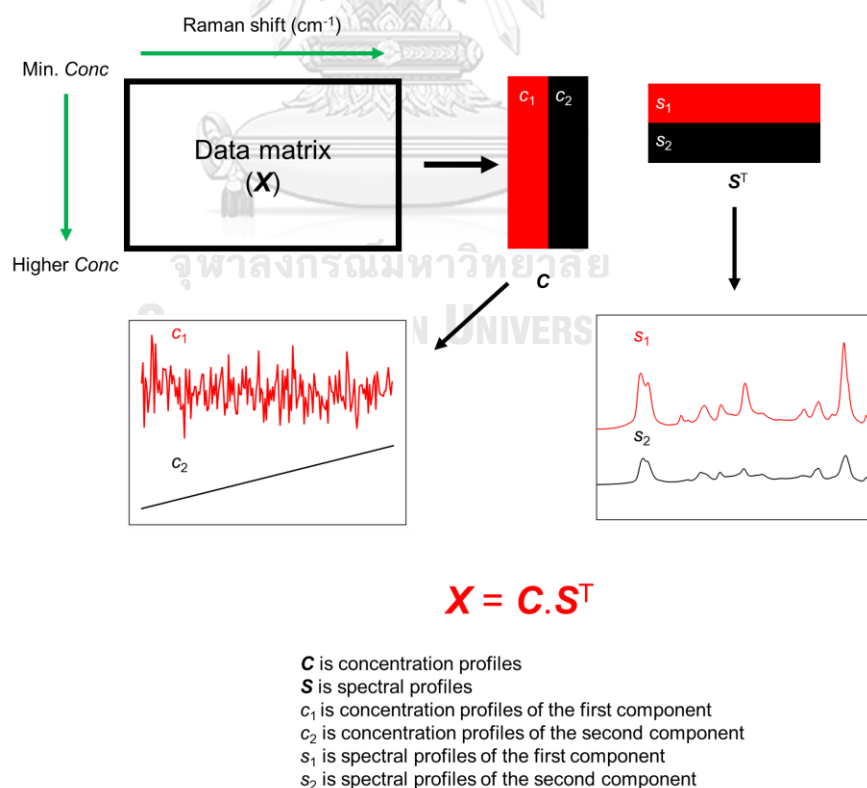


Figure 1.2 Schematic of the MCR-ALS techniques

The main advantages of MCR-ALS are to estimate the bilinear decomposition of mixed experimental data into concentration and absorptivity profiles of the respective chemical species presented in the sample which represents to quantitative and qualitative information, respectively as shown in Figure 1.2. This could increase signal-to noise ratios (S/N ratio) which lead to better visualization of chemical distribution and selectivity which better describes chemical information of each specie⁵¹⁻⁵⁴. Although MCR-ALS models has revealed a highly efficient method to resolve overlapping spectroscopic bands but there are a few works about its application in SERS sensing^{23, 48, 50-51}. A correlation constrained MCR-ALS method was developed to resolve overlapping SERS bands to quantify physiologically relevant concentrations of the bioanalytes in complex media⁵⁰. The standard addition method combined with MCR-ALS were applied to compensate the matrix effects to resolve overlapping bands between uric acid and interference SERS spectra²³. Combination of the high detectability and specificity of the SERS technique with MCR-ALS was used to obtain hyperspectral images to quantify the distribution of polymeric microfilms loaded with paracetamol as an active compound⁴⁸ SERS and MCR-ALS was used as a label-free method to quantify urinary adenosine (a potential cancer biomarker)⁵¹. In most case of SERS detection, the MCR-ALS was mainly used to extract the chemical information of main component and to exclude the signal from interferences (minor components) which might originate from the sample matrix. More cases of the applications of chemometrics method on SERS information are concluded in Table 1.1. As it already discussed in Figure 1.1 that the interferences from capping agent in SERS measurement could be possibly considered as a major component instead of the target analytes. Therefore, the application on MCR-ALS to extract information of the minor components with excluding the main components have not been discussed and discovered.

Table 1.1 Literature reviews of determination of SERS technique combined with chemometric methods

Year	Journal	System	Chemometric	Detection limit	Accuracy	Ref
2014	Chemometrics and Intelligent Laboratory Systems	Thiram combined with <i>p</i> -thiocresol as capping agent to detect	MEM _{SERS} ^a	-	$ARPE^b = 7.5\%$ $RMSEP^c = 0.2$	55
2015	Microchemical Journal	Free labelled paracetamol loaded with polymeric microfilm	MCR-ALS	-	Relative error value = 3.6% %LOF ^d = 8.06%	48
2016	Analyst	Free labelled uric acid in complex matrix	MCR-ALS	LOQ ^e = 0.36 mmol L ⁻¹ LOD = 0.11 mmol L ⁻¹	$R^2 = 0.989$	23
2018	Talanta	Free labelled urinary adenosine	MCR-ALS	LOD = 3.8-4.9 $\mu\text{mol L}^{-1}$	$R^2 = 0.98$	51
2018	LWT - Food Science and Technology	Free labelled chlorpyrifos in tea	GA-PLS ^f	-	$R^2 = 0.98$ $RMSEC^g = 0.28$	56

2020	Analytica Chimica Acta	Free labelled mixture of PAH	MCR-ALS	%LOF = 2.09-2.51	$RMSEP = 0.29$ $R^2 = 0.98-0.99$ $RMSEC = 1.56 - 9.99$	46
2020	Spectrochimica Acta Part A	Free labelled adenine and guanine in complex media	MCR-ALS	-	$R^2 = 0.99$ $RMSEC_{ade} = 0.35$ $RMSEC_{gua} = 0.50$ $RMSEP_{ade} = 0.75$ $RMSEP_{gua} = 0.50$	50
2020	Microchemical Journal	Free labelled docetaxel	CARS-BP-AdaBoost ^b	-	$R^2 = 0.99$ in calibration set $R^2 = 0.97$ in prediction set $RMSEC^i = 0.22$ $RMSEP = 0.25$	57

^a MEM_{SERS} is multiplicative effect model for surface-enhanced Raman spectroscopy

^b $ARPE$ is average relative prediction error = $\frac{1}{N} \sum_{i=1}^N \left| \left(c_{i,1} - \frac{\hat{c}_{i,1}}{c_{i,1}} \right) \right| \times 100\%$

^c $RMSEP$ is root mean square error of prediction

^d %LOF is percentage of lack of fit

^e LOQ is limit of quantitation

^f GA-PLS is genetic algorithm-partial least squares

^g $RMSEC$ is root mean square error of calibration

In this work, we propose an alternative way to enrich the power of MCR-ALS in order to eliminate the signal backgrounds, which is Raman signal from the capping agent, to remain only the analyte information. This methodology involves initially building MCR-ALS models with sample insertion constraint. The constraint is performed by simply adding external spectra of capping agent to obtain the bilinear chemical information of species which is concentration and absorptivity profiles. It starts with low number of added spectra and systematically increasing the number of added spectra until both the estimated quantitative correlation and “lack of fit” of the analyte is satisfactory. The constraint is a crucial step to completely excludes the main signal (from capping agent) from the spectral data. Using this approach, only the chemically relevant specie (even they are minor component) can be determined and might be well matched with the “true” intrinsic Raman profiles. In order to evaluate our methodology, the modified MCR-ALS algorithm was performed on the simulated spectra which were generated by several conditions such as overlapping levels, and the peak intensity ratios (between capping agent and analyte). From the test, it provides some evidences to further support an impact application on the real acquired Raman signal. Then, the developed method was performed on the experimental Raman dataset which involve the detection of carbofuran via diazotization-coupling reaction with *p*-aminothiophenol (*p*-ATP) on silver nanoparticles as SERS substrate.⁵⁵ Using this methodology, MCR-ALS can be more widely utilized by the scientific community for the analysis of SERS data in a data-driven and quantitative platform

1.2 Objective

The objective of this work is developed the chemometric method (MCR-ALS) to extract the analyte signals from SERS spectra to increase the sensitivity and selectivity of the quantification.

1.3 Scope of this work

The MCR-ALS was modified with sample insertion methods. The developed protocol was tested with the simulated spectra generated by using only Gaussian distribution. After validation with the simulated spectra, the efficiency of the developed program was performed on the real SERS spectra on the determination of carbofuran by the azo-dye coupling reaction between carbofuran and *p*-aminothiophenol.



CHAPTER II

THEORITICAL BACKGROUND

2.1 Raman Spectroscopy

Raman spectroscopy is an analytical technique used to reveal chemical fingerprint of target molecule through their vibrational spectrum patterns, while infrared (IR) spectroscopy detects the functional groups of sample molecule. The pattern of IR bands is originated from a change in the dipole moment of a molecule whereas pattern of Raman bands is initiated from a change in the polarizability of the molecule due to the deformation of electric field surrounding the molecule. By measuring the absorbance (or transmittance) of the light which passes through a sample, the frequency of the scattered light usually smaller than the original incident light. This interaction between molecule and incident light is called Stokes scattering, as illustration in Figure 2.1. On the other hand, if the frequency of the scattered light is higher than the incident light, it was called anti-Stokes shift⁵⁶⁻⁵⁷.

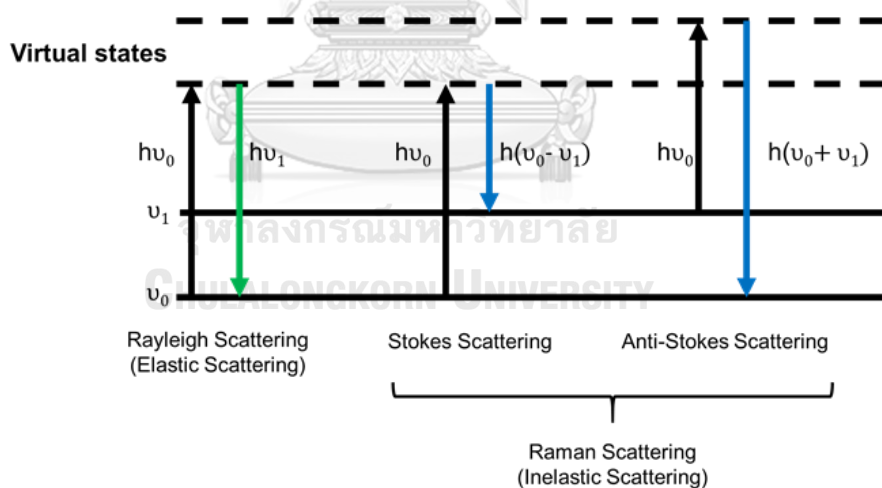


Figure 2.1 Energy level diagram involving Rayleigh scattering and Raman scattering.

The advantages of the Raman spectroscopy are I) The Raman scattering of water and carbon dioxide (CO₂) molecules are weak, which make them not be considered as interference II) Few or not needed in the sample preparation step III) Inexpensive of sample holder or carrier. The Raman spectroscopy can be detecting the signal of the chemical molecule in any phases. However, the low intensity of the scattered light was obtained in the Raman spectroscopy. So, the low concentration of the samples is hard to be operated⁵⁸⁻⁵⁹.

2.2 Localized surface plasmon resonance (LSPR)

The nanostructure of the precise metal (such as Au, Ag, Pt) in the size between 1-100 nm or nanoparticles (NPs) provides some properties with uncommon characteristics, which cannot be detected in the bulk materials, including mechanical, electrical, thermal, chemical and optical properties. To consider the unique optical properties phenomenon, surface plasmon (SP) are involved with delocalized electron oscillation at the surface of metal-dielectric interface. The movement of the oscillating electron can always generate the electromagnetic near-field around the surface of the nanoparticle.

According to the size of the nanoparticles which smaller than the wavelength of incident light, the frequency of incident light probably resonance the natural frequency of electron oscillating on the surface of NPs. This phenomenon called “Localized surface plasmon resonance (LSPR)” which can be locally occurred around the NPs as shown in Figure 2.2⁶⁰. By the plasmon resonance that was generated is depended on the size of the NPs and it can resonance with the matched light source from the Raman laser. The excitation source can be tuned to get the maximum enhancement with the peak of the plasmon resonance. Because of the strong enhancement of surface electric field. The use of Raman spectroscopy combined with LSPR from the metal nanoparticles to enhance the Raman signals. This technique is called “Surface enhanced Raman spectroscopy”

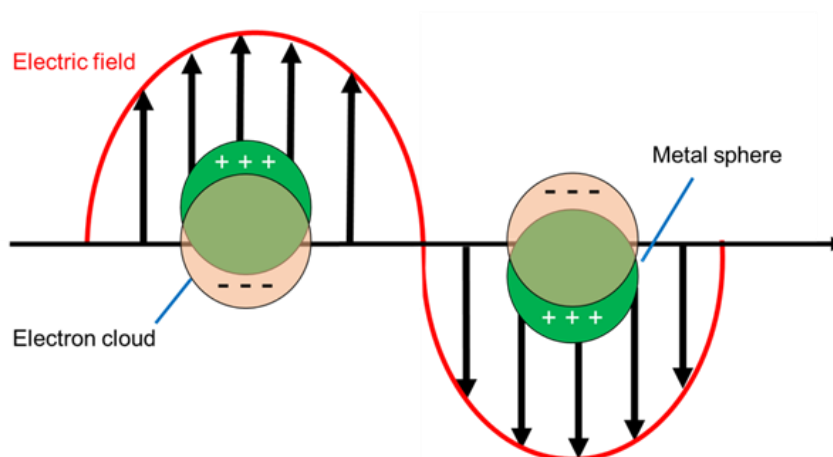


Figure 2.2 Localized surface plasmon resonance (LSPR)

2.3 Surface-enhanced Raman scattering (SERS)

Surface-enhanced Raman scattering (SERS) is a technique which enhances the Raman signal intensity. This technique has widely used in trace analysis to detect the analyte whether it be biomolecule such as tuberculosis⁶¹, chlorpyrifos in tea⁶² or chemical molecules such as polycyclic aromatic hydrocarbon⁶³. By using metal nanoparticles (MNPs), such as silver nanoparticles (AgNPs) or gold nanoparticles (AuNPs), as a SERS substrate. The SERS technique is descending the amplification of the Raman signal by the localized surface plasmon resonance. Depending of the material of the SERS substrate, the electromagnetic enhancement can be calculated to reach factor of $10^{10} - 10^{11}$. Another mechanism involving signal enhancement is chemical enhancement with charge transfer mechanism. The chemical enhancement factors from the charge transfer are up to 10^3 . The SERS can be used to detect the analyte molecules by depositing them on the surface of the MNPs which generate the intense electromagnetic fields. This phenomenon leads to the enhancement capability of Raman measurement when the target molecules are in “hot spot” of nanoparticles. The high sensitivity and the selectivity of the SERS was obtained and could be increased by modified the surface of the nanoparticles to induce the analyte molecules immobilizing closely the hotspot⁶⁴⁻⁶⁵. The hot spot in the SERS technique is generally located between the gap of the MNPs that was used as the SERS substrate. The area of hot spot and the enhancement factor of the hot spot is shown in Figure 2.3. The hot spot is related with the enhancement ability. If the gap of the MNPs is closet in the

range of sub-nanoscale (2-20nm), the signal of SERS is highest enhanced. So, the closer of the analyte molecules within the hot spot, the higher obtained SERS signal

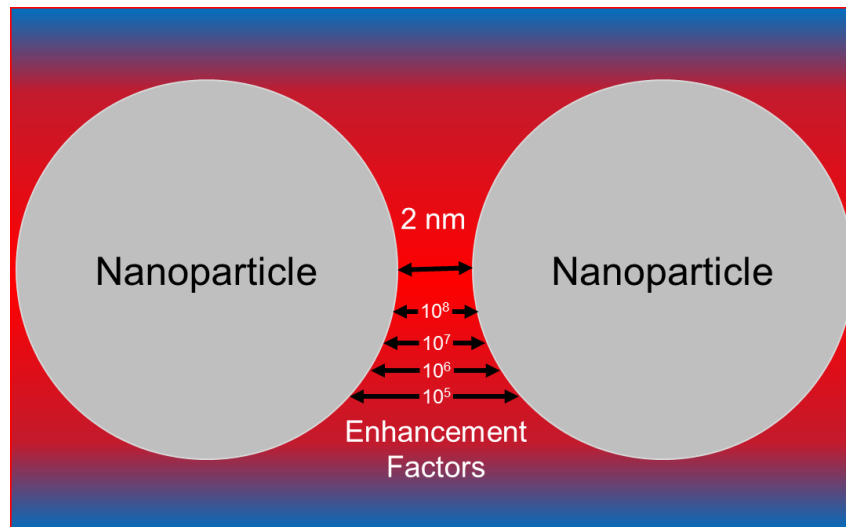


Figure 2.3 Illustration of a hot spot generated by the gap of the nanoparticles. The SERS enhancement related with the gap size of the connected nanoparticles

2.4 Multivariate Curve Resolution-Alternative Least Square (MCR-ALS)

Multivariate curve resolution-alternative least square (MCR-ALS) is an iterative algorithm that can solve the mixture analysis problem into the pure contributions from the individual information of an original data matrix of the mixed measurement. The multicomponent data set (\mathbf{X}) consisting of r rows of wavelength (nm) or spectral channels and c column of samples.

$$\mathbf{X} = \begin{bmatrix} x_{1,1} & x_{1,2} \dots & x_{1,nc} \\ x_{2,1} & x_{2,2} \dots & x_{2,nc} \\ \vdots & \vdots & \vdots \\ x_{nr,1} & x_{nr,2} & x_{nr,nc} \end{bmatrix} \quad 2.1$$

The symbol $x_{i,j}$ represent the data point represents the data point associated with i^{th} and j^{th} column of the matrix

In the spectroscopy technique, the absorbance data can be explained with the Beer Lambert's law. So, the data point ($x_{i,j}$) of the spectroscopic can be extracted in terms of the absorptivity ($s_{i,j}$) and the concentration ($c_{i,j}$). The $x_{i,j}$ can be expressed as:

$$x_{i,j} = \sum_{k=1}^n c_{k,j} s_{i,k}^T + e_{i,j} \quad 2.2$$

Where $e_{i,j}$ is the noise of the data matrix.

From the eqs 2.2 the classical equation of the MCR-ALS of the bilinear data model including concentration profiles (C) and pure spectra profiles (S) is shown in general matrix form (eqs 2.3). By the overall process was shown in Figure 1.2.

$$X = CS^T + E \quad 2.3$$

When E is the error or variance matrix

The steps of the MCR-ALS algorithm are detailed⁶⁷

1. Determinations of the number of components

The number of components of the data set can be known or determined from principal component analysis (PCA). The MCR-ALS and PCA methods describing by the variance to consider the number of the components. By the first rank chemical component is the maximum of the variance value. In this work, only one component which might relate to capping agent was selected and extracted from the MCR-ALS algorithm.

2. Generation of initial estimates of C or S^T

Initial estimates in MCR-ALS can be concentration profile or pure spectra. Normally, the initial estimates are the profiles of the components that want to be recovery. It can be based on the previous knowledge, such as, the spectra of the component in data set, spectra at maximum chromatographic peaks. In this work, the mean spectra of the capping agent were selected to the initial estimates of the pure spectrum.

3. Iterative alternating least square optimization of C and S^T under constraint until convergence is achieved

The constraints are the essential part of the MCR-ALS algorithm. The beneficial of the constraint are 1) introducing chemical and mathematical information to afford the chemical meaning to the concentration profiles and the pure spectra and 2) suppressing the ambiguity related to the MCR solutions. The most common and applicable constraints in MCR-ALS are non-negativity, unimodality, closure, selectivity and local rank, and equality constraints. In this work, the non-negative least square (nnls)⁶⁸ was selected, due to the non-negativity of the output spectra are similar as spectroscopic spectra⁶⁷.

The nnls constraint was calculated the coefficients (a) are not allowed to become negative. The argument of the nnls can be written form

$$\begin{aligned} \min \|Xa - Y\|_2 & \quad 2.4 \\ \text{Subject to } a \geq 0 & \end{aligned}$$

Where the X is intensity of the spectroscopic data in $m \times n$ dimension, Y is response in m dimension, a is coefficient, min is argument to minimize the calculation, and $\| \cdot \|$ is the Euclidean norm denotes.

From the eqs 2.4, the spectroscopic spectra were forced to the non-negative values in both the concentration and pure spectra profiles. The negative values were forced to zero with this constraint. It should be avoided in certain kinds of spectroscopic profiles that provide some of negative values or when working with the derivative spectra. So, the nnls be appropriate to use in this work due to the subtraction of the stronger signal⁶⁸.

The MCR-ALS algorithm that was used is MCR-ALS toolbox (version GUI 2.0)⁶⁹. This GUI perform under MATLAB (version R2018a).

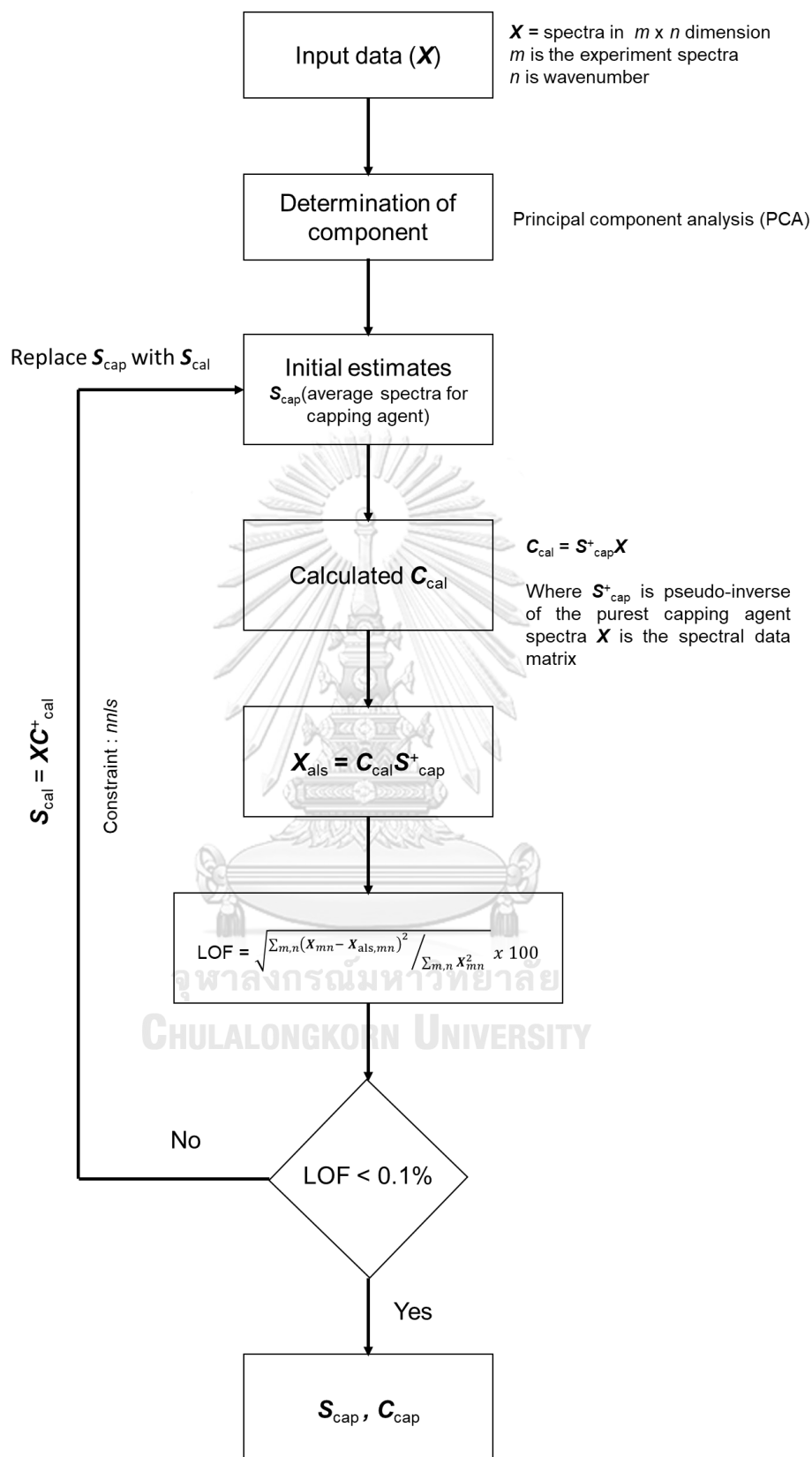


Figure 2.4 Scheme of the step of MCR-ALS GUI that was used in this work

CHAPTER III

EXPERIMENTAL SECTION

3.1 Spectrum simulation

In order to elucidate the features and reliability of MCR-ALS with sample insertion constraint, the proposed method was performed on the series of simulated spectra. The pure spectra with independent peaks and intensity variations are generated using a Gaussian function⁷⁰.

$$F(x) = \frac{A}{\sigma\sqrt{2\pi}} e^{-\frac{(v-\mu)^2}{2\sigma^2}} \quad (3.1)$$

Where A , v , μ , and σ are the peak intensity, spectral variables, peak position, and standard deviation, respectively. Generally, the parameter values especially peak position and peak width could be assigned to any values, but they were adjusted to be closet in the range of real Raman spectra. The peak position of the capping agent was fixed at 1715 cm^{-1} , the peak width of the capping agent and the analyte were fixed at 75 and 45, respectively. The peak position of the analyte was varied from 1632, 1671, 1687, 1700, and 1715 cm^{-1} . It has been assumed that peak intensity (A) only depends on a function of wavenumber (Raman shift). Each spectrum consists of two independent peaks which represent the Raman signal of a capping agent and a target analyte, respectively. The spectrum was modified closet to the real Raman spectral peaks by adjusting different overlapping conditions and intensity ratios between the analyte and the capping agent.

The resolution (RS) between the two peaks was adjusted to be 0 (completely overlap) to 1.5 (non-overlap). The value of RS is directly corresponding to the overlapping level of the two peaks. By the RS values were calculated by eqs 3.2

$$RS = \frac{2(p_{ana} - p_{cap})}{(w_{ana} + w_{cap})} \quad (3.2)$$

When p_{ana} is peak position of the analyte, p_{cap} is peak position of the capping agent, w_{ana} is width of the analyte peak, and w_{cap} is width of the capping agent peak.

The value of RS is directly corresponding to the overlapping level of these two peaks. The higher value of RS , the lower overlapping level. On the other hand, the low RS value express the high overlapping level of these two peaks. The overlapping level and the combined peaks at different RS values are shown in Figure 3.1. The position of the analyte peak was changed by the vary of the mean values of the analyte signal at 1632 ($RS = 1.5$), 1671 ($RS = 0.8$), 1687 ($RS = 0.5$), 1700 ($RS = 0.2$), and 1715 ($RS = 0$), while the peak position of capping agent equal to 1715.

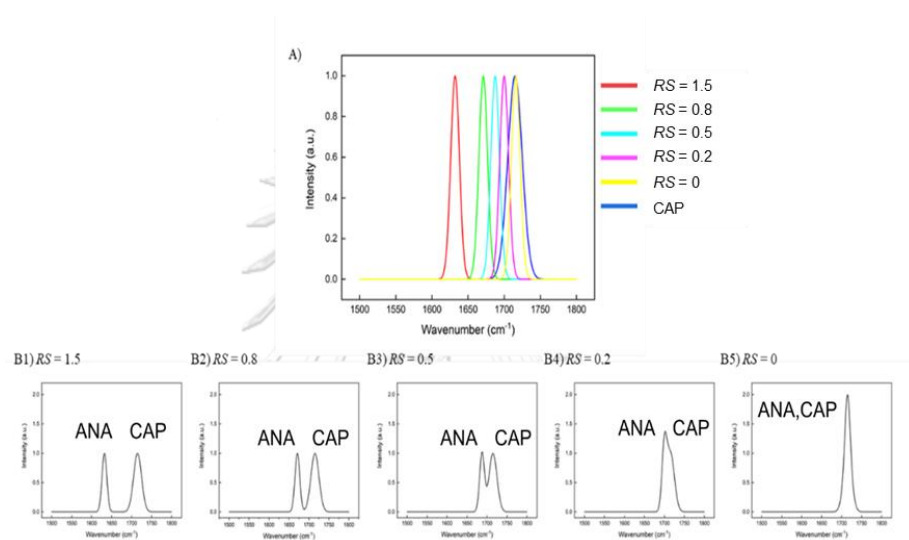


Figure 3.1 (A) pure spectra of analyte (s_{ana}) at the different RS values compared with pure spectra of capping agent (s_{cap}) (blue line) when the red, green, cyan, purple, and yellow line represent the s_{ana} at $RS = 1.5, 0.8, 0.5, 0.2$, and 0 , respectively. (B1) – (B5) the combined of s_{ana} and s_{cap} at the RS values = $1.5, 0.8, 0.5, 0.2$, and 0 , respectively. The decrease of the RS values the peak of the analyte moved closer to the peak of the capping agent and more overlapped. ANA and CAP are represent analyte and capping agent, respectively.

The simulated spectra of capping agent (X_{cap}) can be computed by the multiplication of concentration vector of capping agent (c_{cap}) with %RSD is 10% by simulated concentration profiles of capping agent with 10% of capping agent concentration using normal distribution calculated. The eqs of the %RSD as

$$F(x) = \frac{1}{\sigma\sqrt{2\pi}} e^{-\frac{(v-m)^2}{2\sigma^2}} \quad (3.3)$$

While m is mean = 500 and σ is standard deviation = 10%

while the spectra of an analyte (X_{ana}) were computed by multiplication of concentration (c_{ana}) and the pure spectra (s_{ana}) as shown below. In our case, the concentration value of analyte was constantly constrained without any added %RSD.

$$X_{cap} = c_{cap} \cdot s_{cap} \text{ and } X_{ana} = c_{ana} \cdot s_{ana} \quad (3.4)$$

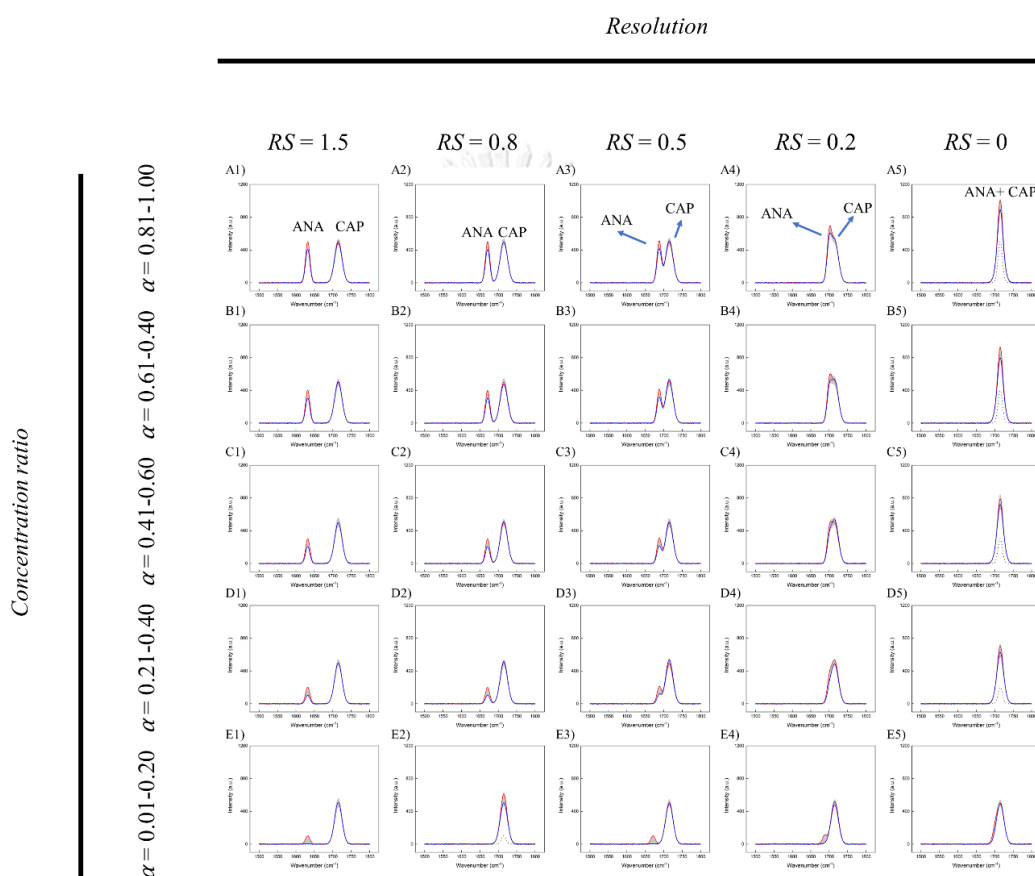


Figure 3.2 The simulated spectra from A) – E) the ratio of the concentration of the analyte were varied form 0.01-0.20, 0.21-0.40, 0.41-0.60, 0.61-0.80, and 0.81-1.00 and 1) - 5) the RS values were varied from 1.5, 0.8, 0.5, 0.2, and 0, respectively. The red, blue and grey line represent the highest, lowest and moderate concentration of the analyte. ANA and CAP represent the analyte and capping agent peaks, respectively.

Moreover, the intensity ratio between the analyte was set to 0.01- 1.5 compared to the intensity of the capping agent. To simplify the definition, the

intensity ratio of 0.01 refer to the average intensity of the analyte is approximately 1% compared to the average intensity of the capping agent.

Despite to SERS, it is a scattering technique, therefore, it normally provides some fluctuated SERS signals with %RSD between 1-10%. In simulated spectra, the %RSD of the signal from capping agent was adjusted to 10%. In the last step, the 0.5% of the random noise was added to the spectra in order to include part of non-linear in the synthetic spectra (the random light scattering from the small particle and external rays). The random noises were estimated from the baseline intensity of polystyrene as a reference. The simulated spectra of two independent peaks with different overlapping levels and different intensity ratio are shown in Figure 3.2

3.2 Removal of Main components in SERS signal

In SERS signal, the traces of analytes can be hidden by the major species, particularly corresponds to the large amount of surface capping agent on the metal surface. However, because of their relative abundance, the SERS signal of major species are difficult to be determined and removed to remain only the signal from the traces. This goal of the data analysis is to pursue with uses of MCR-ALS techniques^{23, 50-51}. The method assumes that each spectrum can be described as a bilinear combination of the signal of pure component spectra (\mathbf{S}) and its concentration (\mathbf{C}). The relationship can be written as.

$$\mathbf{X} = \mathbf{C} \cdot \mathbf{S}^T + \mathbf{E} \quad (3.5)$$

Where the data matrix \mathbf{X} (set of Raman spectra) with rows corresponding to sample and columns corresponding to the Raman shift (cm^{-1}), \mathbf{C} is the concentration profiles of all species detected, and \mathbf{S} is representing their pure spectral profiles. At the beginning of the MCR-ALS original algorithm, the first guess of the concentration or the spectral profiles was estimated for each component. In the study, a first guess on the pure spectra and then the concentration profile can be estimated by the pseudoinverse as follows:

$$\hat{\mathbf{C}} = \mathbf{X} \cdot \hat{\mathbf{S}}^T \cdot (\hat{\mathbf{S}} \cdot \hat{\mathbf{S}}^T)^{-1} \quad (3.6)$$

and in turn, the concentration matrix \mathbf{C} can be updated to

$$\hat{\mathbf{S}} = (\hat{\mathbf{C}}^T \cdot \hat{\mathbf{C}})^{-1} \cdot \hat{\mathbf{C}}^T \cdot \mathbf{X} \quad (3.7)$$

Where $\hat{\mathbf{S}}$ and $\hat{\mathbf{C}}$ are the estimates and the T symbol denotes as transposition. The ALS algorithm iterates between eqs 3.6 and 3.7 until reconstructed matrix from the estimates minimize the error between and calculated $\hat{\mathbf{X}} (= \hat{\mathbf{C}} \cdot \hat{\mathbf{S}}^T)$ and original data matrix \mathbf{X} . During the ALS calculation, a non-negative least square (*npls*)⁶⁸ constraints of both concentration and pure spectrum profiles are also performed.

In the case under investigation, the goal is simpler because \mathbf{X} is largely dominated by the presence of a single compound (capping agent on the metal surface) that is required to be modelled and removed and that appears as a very strong signal compared to the signal from the analyte. Therefore, the initial rank is determined as 1, a guess of the spectral profile (average spectrum of capping agent) is taken as the initial profile of the most abundant signal in Raman spectrum. Calculation on eqs. 3.6 and 3.7 will leads to a $\hat{\mathbf{C}}_{\text{cap}}$ and $\hat{\mathbf{S}}_{\text{cap}}$ which characterize as the major component of capping agent in the case. The principal of the developed method is to seek for pure vectors of capping agent and then subtracted from the original data matrix to remain only the analyte signal (\mathbf{X}_{ana}) calculated as

$$\hat{\mathbf{X}}_{\text{ana}} = \hat{\mathbf{X}} - \mathbf{c}_{\text{cap}} \cdot \mathbf{s}_{\text{cap}}^T \quad (3.8)$$

It should be noted that some of the information held in \mathbf{X}_{ana} may still relate to some residual interferences. However, if the capping agent signal was not completely removed, this will strongly disturb the underlying quantitative information of the analyte signal. To completely exclude the capping agent signal, an additional constraint of sample insertion is applied. The external spectra of capping agent (\mathbf{X}_{cap}) was added to the data matrix \mathbf{X} to obtain $\mathbf{X}_c (= [\mathbf{X}; \mathbf{X}_{\text{cap}}])$ prior to perform MCR-ALS. The generated \mathbf{X}_c were used instead of \mathbf{X} in the iterative eqs 3.6 and 3.7 until it converges. The number of added spectra is monitored to reveal the completely elimination of capping agent signal. Since \mathbf{X}_{ana} has been extracted, it is used to build models of univariate calibration directly from the extracted spectra. In the case, a calibration curve is individually built for each set of samples after including known analyte concentration. The intensity of the analyte is plotted against its concentrations, thereby obtaining the standard calibration curve used to calculate the analyte concentration in an unknown sample.

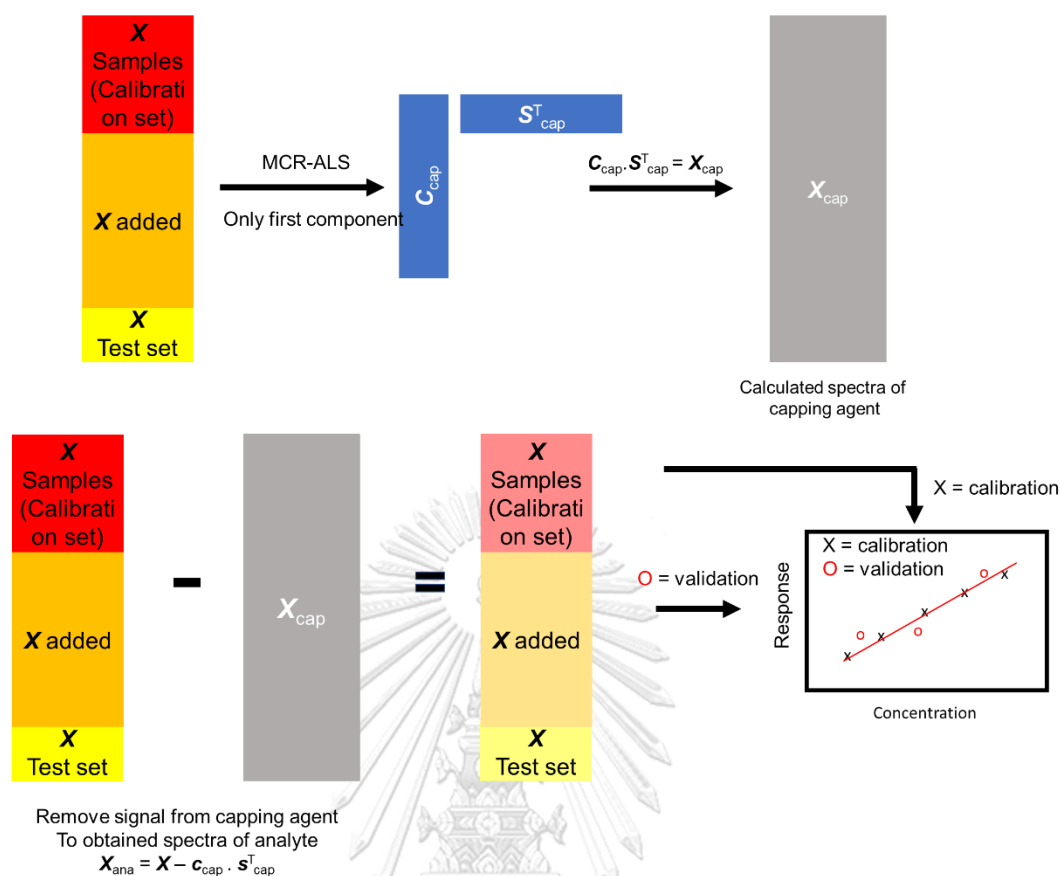


Figure 3.3 Scheme describe the extraction of capping agent signal by using sample insertion constraint with MCR-ALS method and Remove the signal of capping agent and construct the standard calibration curve from the analyte signal which then is used to predict the test samples

This protocol provides the capability to predict analyte concentration even in the presence of unknown interferences. Thus, the identification of the interferences is not required as SERS with capping agent is already designed to be selective to the target analyte. Moreover, the calibration and test samples can be either arranged in the same matrix or the different matrix before applying the MCR-ALS algorithm. The correlation coefficient (R^2) and the Mean average percentage error ($MAPE$) was used to evaluate the calibration model. In this work, multivariate data analysis was performed using MATLAB (version R2018a) and MCR-ALS toolbox (version GUI 2.0)⁶⁹. The overall calculation scheme is displayed in Figure.3.3.

3.3 Performance Indices

The R^2 and $MAPE$ values were used to evaluate the calculation model. The R^2 value was calculated the coefficient of the determination by proportion of the variance in the dependent variable that is predictable from the independent variables. The relation of the intensity and presetting concentration. The higher value of the R^2 value (close to 1) shows the small differences and unbiased between the preset values and the predicted values. Unbiased means that the fitted values are not systematically too high or too low in the observation space.

The $MAPE$ value was calculated the difference between the predicted concentration ($Conc_{cal}$) and the presetting concentration ($Conc_{pre}$) by the $MAPE$ value was calculated from the absolute subtraction between the predicted concentration and the presetting concentration divided by presetting concentration. After that multiply by 100 and average this value, it can be written as follow.

$$MAPE = \frac{1}{n} \sum_1^n \left| \frac{Conc_{cal} - Conc_{pre}}{Conc_{pre}} \right| \times 100 \quad (3.9)$$

The predicted concentration was calculated by linear regression equation the intensity of analyte plot with presetting concentration can be written as follow.

$$\text{Intensity} = \text{slope} \times \text{concentration} + \text{intercept} \quad (3.10)$$

When, intercept and slope were obtained from the calibration curve.

In the part of the real system, the root-mean-square error ($RMSE$) value was reveals difference between the predicted concentration and the presetting concentration. The $RMSE$ value was calculated by square root of the mean of square value of difference between predicted concentration and actual concentration. It can be written as follow

$$RMSE = \sqrt{\sum_1^n \frac{(Conc_{cal} - Conc_{pre})^2}{n}} \quad (3.11)$$

The lower of the $RMSE$ value refer to the smaller error of the concentration prediction

The Euclidean distance used to reveal the similarity of the extracted capping agent spectra and the pure capping agent spectra. It can calculate the distance between

two datasets of the observed capping agent spectra (S_{obs}) that were obtained from the calculation and the capping agent spectra (X_{cap}). By the Euclidean distance calculation from equation 3.12

$$\text{Euclidean Distance} = (X_n - S_n)(X_n - S_n)^T \quad (3.12)$$

When, n is spectra. The lower value of the Euclidean distance (close to 0) shows the higher similarity of the extracted pure capping agent spectra and the capping agent spectra

3.4 Real system (quantify carbofuran using SERS)

The detection of carbofuran through the diazotization-coupling reaction was used as a real experimental SERS system. Briefly, silver nanoparticles (AgNPs) as SERS substrate were prepared by conventional procedure⁷¹. The reduction of AgNO_3 with $\text{Na}_3\text{C}_6\text{H}_5\text{O}_7$ was occurred to obtain the uniform AgNPs with in-plane plasmon resonance band at 450 nm indicating an average size of approximately 50 nm.⁵⁵ Prior to SERS measurement, carbofuran was converted to carbofuran phenol by hydrolysis reaction. The hydrolysis reaction was prepared by diluting carbofuran by KOH solution and then was incubated at 50°C for 3 hours to obtain carbofuran phenol. In another batch, diazonium ion was prepared by adding 5% NaNO_2 into a solution of *p*-ATP in HCl at 0°C for 1 min. The diazonium coupling reaction was immediately attained by mixing with the solution with the carbofuran phenol in alkaline condition at 0°C for 1 min. After the diazo-coupling reaction, each sample was combined with silver colloid solution for 5 min. The mixture was dropped on a virgin aluminum plate. SERS spectra were collected using a DXR Raman microscope (Thermo Scientific) with a 780-nm excitation laser of 14 mW laser power. The signal acquisition was operated under a 10X-objective lens with a laser spot of 3.1 μm . SERS spectra were obtained using a 2-sec exposure time with 8 accumulations. The details of experiment were described elsewhere⁵⁵. The overview scheme of SERS measurement of carbofuran through diazo-coupling reaction with *p*-ATP when AgNPs colloidal solution was used as SERS substrate is demonstrated in Figure 3.4

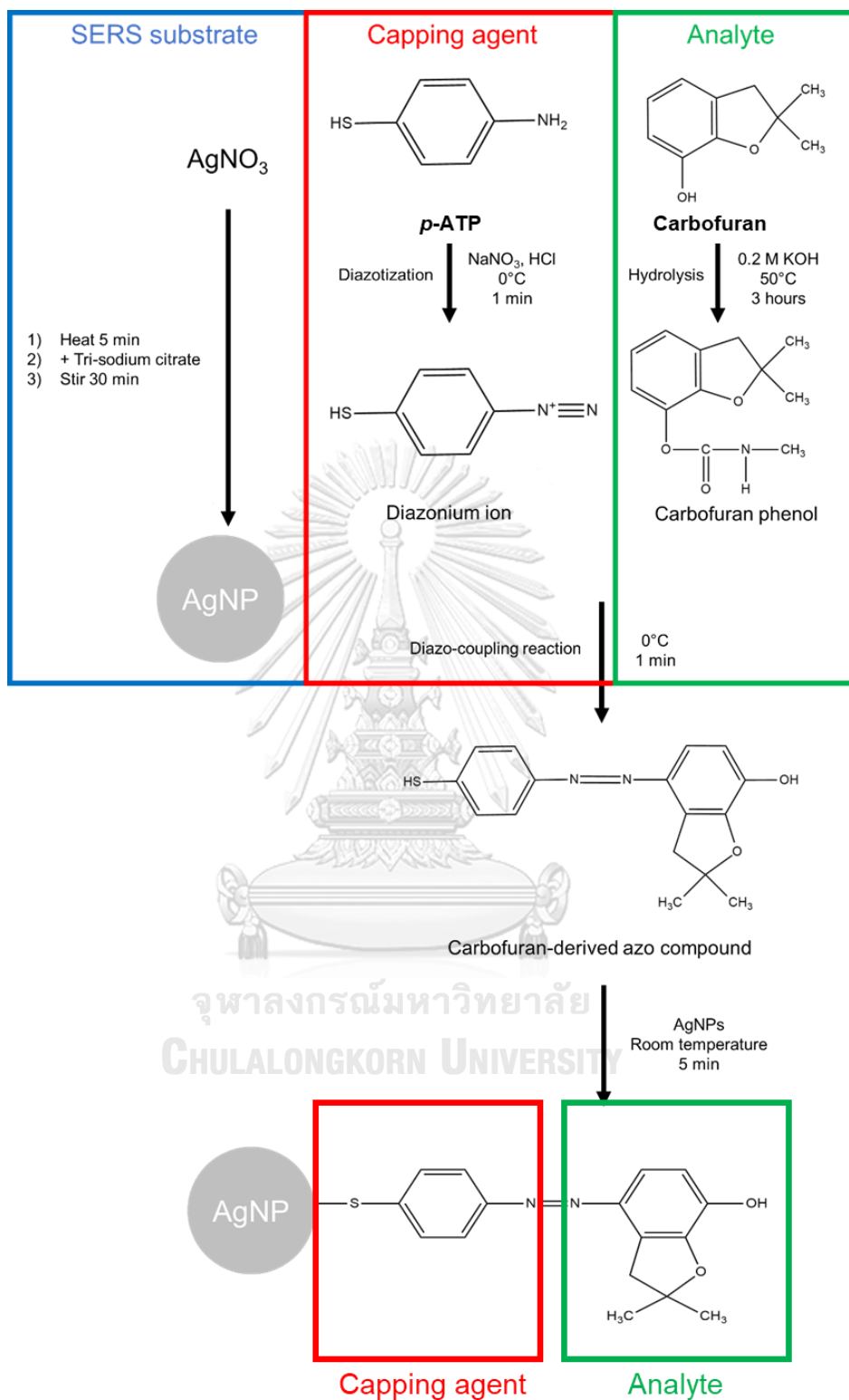


Figure 3.4 SERS measurement of carbofuran via diazo-coupling reaction with *p*-ATP when AgNPs colloid is used as SERS substrate

CHAPTER IV

RESULTS AND DISCUSSION

4.1 Spectral simulation

Three different criteria involving background subtraction, classical MCR-ALS and MCR-ALS with sample insertion constraint were performed on the simulated datasets with different overlapping levels at the various intensity ratios. The calibration curve was constructed similar to a univariate calibration involving intensity and concentration of the analyte peak. The index of R^2 value was used to estimate the prediction accuracy of the calibration curve generated by the three criteria. The contour mapping of R^2 value at different RS and different intensity ratios are shown in Figure 4.1A. The contour areas with grey color reveal the calibration curve with satisfied R^2 (> 0.99) while yellow-red color represent badly prediction accuracy ($R^2 < 0.5$).

In case of using background subtraction, the expected results of the R^2 value are satisfactory when RS is higher than 0.5. However, the R^2 value is improper when RS is lower than 0.3 (badly overlapped peaks). By using original MCR-ALS, the peak of analyte considered as minor component could not be possibly extracted as the R^2 values of the calibration curve are unsatisfied in all cases (R^2 value < 0.3). Based on the theory, the MCR-ALS could not appropriately be used to monitor either the interferences or a minor component (an analyte in the case) in the system.

To improve the prediction, the sample insertion criterion was modified in the beginning step of MCR-ALS calculation. In order to completely remove the capping agent peaks considered as a major component, the virgin spectra of this capping specie should be much higher than the set of mixture spectra. Therefore, MCR-ALS could identify them as the first rank component utterly. By using the sample insertion criteria, it can be seen that the R^2 value is dramatically improved and is acceptable in all conditions especially when the peaks are highly overlapped ($RS < 0.5$). Figure 4.1B shows the calibration plot of the condition at position (I)-(V) on the contour map of R^2

value (Figure 4.1A). From the scatter plots, it can be clearly seen that the calibration curve produced by using MCR-ALS modified with sample insertion constraint is noticeably improved especially in the case of low *RS* (high overlapped conditions). The scatter plot of the analyte signal and concentration shows the good correlation compared with the other criteria. This suggests that the sample insertion constraint is crucial and necessary to be applied with MCR-ALS calculation in order to completely exclude the dominate unnecessary large peak. Inset Figures show the extracted analyte peak after the capping agent peak was removed by the three criteria. By classical MCR-ALS, it could be clearly seen that the combination peaks between capping agent and analyte were occurred, while the analyte peak was completely isolated by using the MCR-ALS modified by sample insertion constrain. The number of added capping agent spectra in each condition was optimized as shown in Figure 4.2A1.

In this section, the number of spectrum (of capping agent) required to be inserted in the MCR-ALS calculation is monitored, optimized and investigated. The extra set of the capping agent spectra were added as the constraint with the ratio of the number of capping agent spectra divided by the number of calibration spectra between 2-100 times. An appropriate ratio of the added capping agent spectra was automatically determined by the change of mean absolute percentage error (*MAPE*) which is less than 5% as follows.

$$\frac{MAPE_i - MAPE_{i-1}}{MAPE_{i-1}} \times 100 < 5$$

Where *i* is the step of ratio.

The indicator of *MAPE* was used instead of root mean square error (*RMSE*) because *MAPE* could be calculated in term of percentage. In the data simulation, the peak intensity is shown in arbitrary unit (a.u.), therefore, the *MAPE* index is more appropriated rather than *RMSE* which was normally used to display the actual value.

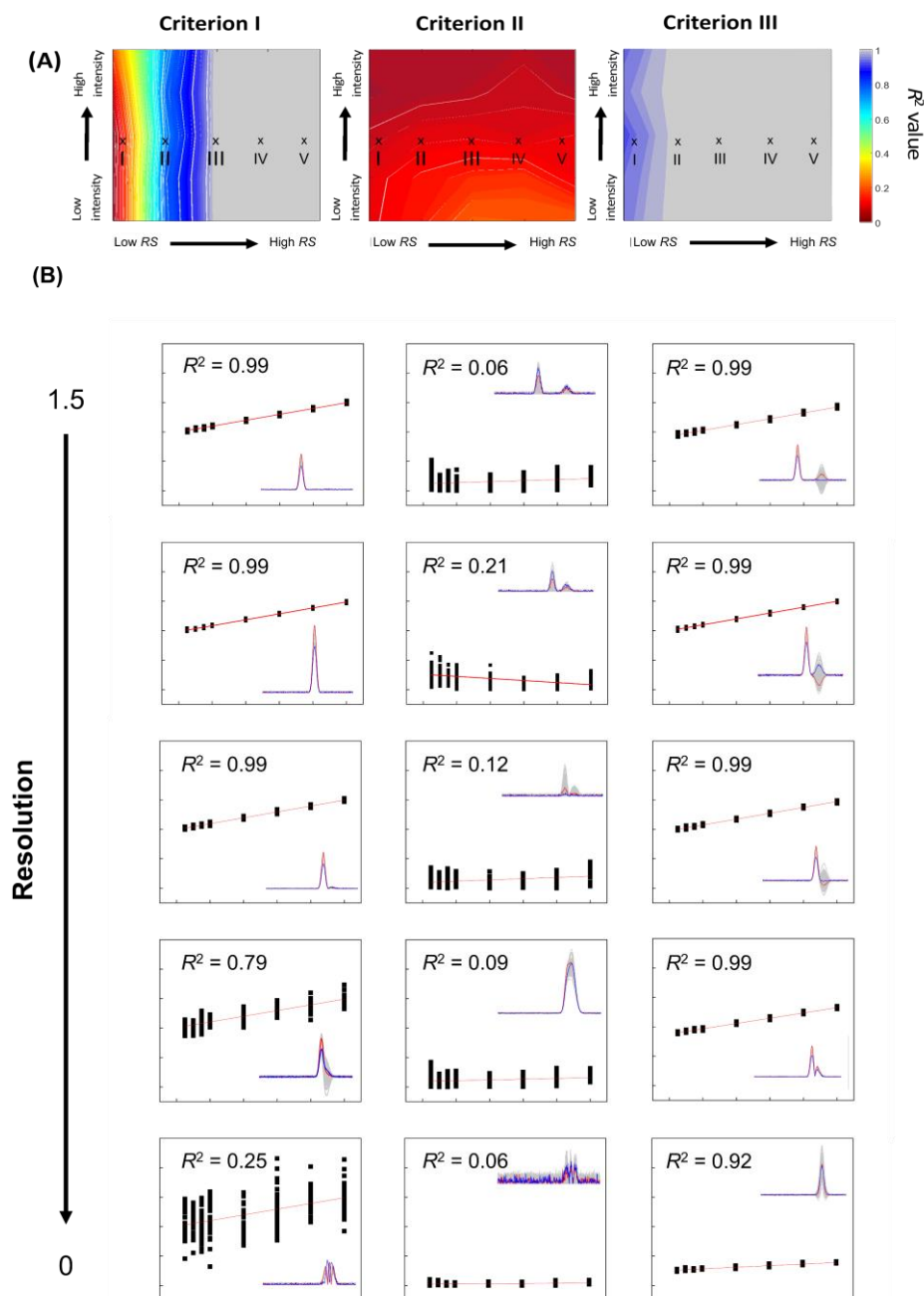


Figure 4.1(A) The contour map of R^2 value of the calibration curve calculated from analyte peak extracted by criterion (I) background subtraction, (II) MCR-ALS and (III) MCR-ALS with sample insertion constrain. **(B)** the calibration curve plot from point (I), (II), (III), (IV), and (V) on the contour map with the inset Figures as the analyte peak after extraction. All Figures are in the same scale of intensity and concentration (a.u.). Scatter plot of the RS = 0 and 0.20 were shown in APPENDIX

Figure 4.2A1 shows the mapping of the sample ratio which appropriately added to the data matrix in order to completely eliminate the capping agent peak. Surprisingly, the number of added samples is not strongly related to the overlapping levels, but the added ratio tends to significantly increase when the intensity ratio is high. This observation suggests that the system contains the target analyte with large peak intensity, it requires more added capping spectra. On the other hand, only small amount of adding spectra is needed for the system with low peak intensity of the analyte. The relation of intensity ratio of the analyte might be strongly correlated to the selection of the chemical rank. In the developed algorithm, the signal from the capping agent should be selected as the first chemical rank as it will further be eliminated in the next calculation step. However, if the intensity ratio of the analyte is approximately close to the peak intensity of the capping agent, it is possible that the capping agent could not be determined as the first chemical rank. Therefore, the added number of capping agent spectra should be increased in the simulated data with high peak intensity ratio of the analyte. After the number of added spectra was determined, the prediction accuracy from the calibration set and the validation set was revealed in term of *MAPE* values shown in Figure 4.2A2 - 4.2A3.

From *MAPE* map, they show that most of the conditions give the acceptable percentage error of prediction ($MAPE < 10$) in both calibration and validation sets. To get the insight information, the scatter plots of the predictive concentrations against the actual concentrations at various conditions, e.g. $RS = 0, 0.2$ and 0.5 with intensity ratio of 0.5 was shown in Figure 4.2B1 – 4.2B3. The results were extracted by using the optimized added samples of capping agent spectra shown in Figure 4.2A1. In the scatter plots, the black circle plot represents the results from the calibration model and the red circle demonstrates the prediction of the validation set. In case of $RS > 0$, fulfilled R^2 value of the prediction from calibration and validation is higher than 0.99 . The spectra shown in inset Figures display the original simulated spectra of calibration set (black), the simulated spectra for validation set (grey), the extracted spectra of calibration set (blue) and the extracted spectra of validation set (red), respectively.

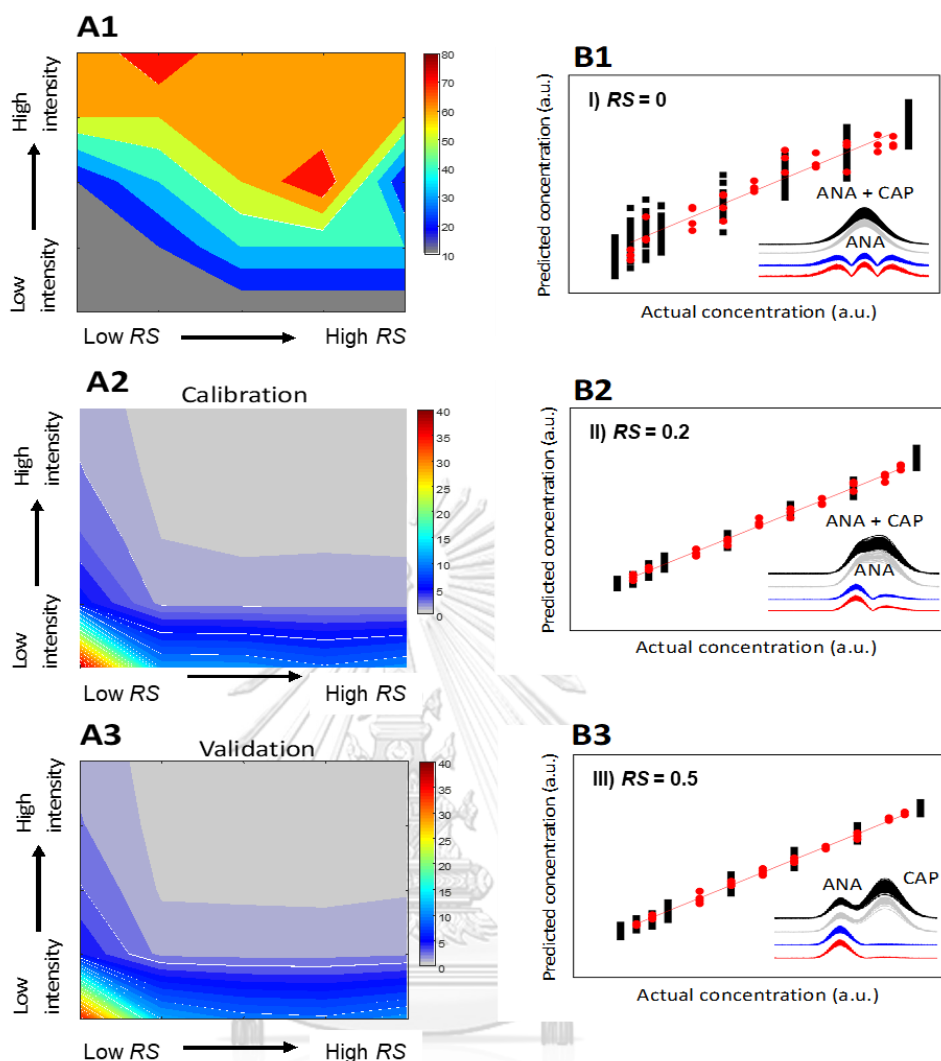


Figure 4.2 (A1) The contour map of the sample ratio appropriately added to the data matrix to completely removed the capping agent peak. The map of mean absolute percentage error (MAPE) of calibration set (A2) and validation set (A3) at different conditions. (B1-B3) Plot of the MCR-ALS predicted concentrations versus actual concentrations using the sample insertion constraint for $RS = 0, 0.2$ and 0.5 respectively. Inset Figures of B1-B3 demonstrate the original simulated spectra of calibration set (black), the simulated spectra for validation set (grey), the extracted spectra of calibration set (blue) and the extracted spectra of validation set (red).

The dissimilarity of the capping agent and the extracted spectra at the different number of added capping agent spectra were shown in the Figure 4.3. The dissimilarity between the preset spectra and the extracted spectra of the capping agent was calculated using the Euclidean distance at the $RS = 0.5$. From the Figure 4.3A, the dissimilarity of the preset and the extracted spectra of the capping agent were decreased when the number of the added spectra were increased. The dissimilarity was insignificantly changed when the number of added capping agent spectra are larger than 40 times compared to the number of the analyte spectra. Figure 4.3B-F shows the pure spectra and the extracted pure spectra of the capping agent from the condition of $RS = 0.5$ at the sample ratio of 10, 40 and 100 times. From the inset Figure, the differences between the preset spectra and the extracted spectra are small at the lowest analyte concentration (Figure 4.3B) compared with the condition of high concentration ratio (Figure 4.3F). For condition with low concentration ratio, only 10 times of sample insertion is adequate for MCR-ALS to extract the pure spectra of capping agent, while 100 times of sample insertion ratio is required for the system with high concentration ratio. From the observations, it confirms that the number of added spectra strongly affect the determination of the chemical rank in the system. High number of capping agent spectra in the system tend to provide the first chemical rank of the capping agent to be extracted. Therefore, the smaller number of added spectra for the system with low concentration ratio is required, while the larger number of added spectra is necessary when the concentration ratio is getting larger.

The results express that the capping agent peaks was completely eliminated from both calibration set, and validation set when the appropriate number of capping agent spectra was added as constraint in MCR-ALS calculation. The developed method is very powerful as it can solve even the spectra with very high overlapped peaks ($RS \sim 0$). Furthermore, the method is fully automating on either generate set of capping agent spectra or optimize the appropriate number of added spectra. From this section, it is now ready to elucidate the performance of developed method with the real experimental spectra on SERS measurement.

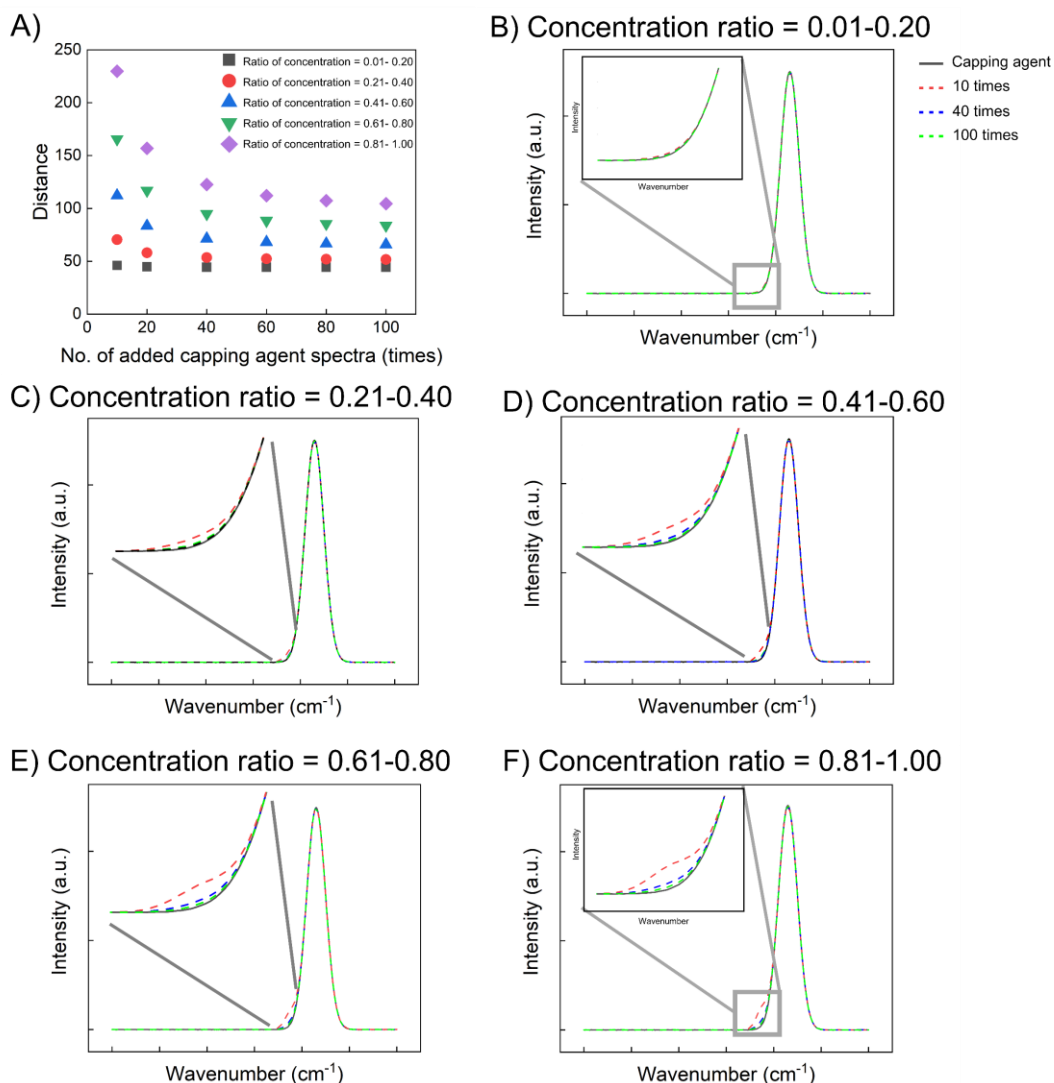


Figure 4.3 (A) The Euclidean distance of the preset spectra and the extracted spectra of capping agent at the various number of the added capping agent. The black square, red circle, blue triangle, green triangle, and purple diamond are the distance at the different concentration ratios from 0.01-0.20, 0.21-0.40, 0.41-0.60, 0.61-0.80, and 0.81-1.00, respectively. **(B)** the preset spectra (black line) and the extracted spectra of the capping agent using sample insertion at 10 (red dash line), 40 (blue dash line) and 100 (green dash line) times, respectively. The inset Figures show the spectra at the 1700 cm^{-1} with condition of $RS = 0.5$.

4.2 Real system (quantify carbofuran using SERS)

The detection of carbofuran using the diazotization-coupling reaction between *p*-ATP (capping agent) on the AgNPs and derivative of carbofuran phenol (target analyte) was used as a real experimental SERS system. Figure 4.4 shows the SERS spectra of the diazonium ion and the carbofuran-derived azo compounds on AgNPs as SERS substrate. The peaks at 1075, 1327, 1429 and 1570 cm^{-1} represent the typical bands of C-S stretching, CCH, NCC (phenyl-N) in-plane bending, C-H and O-H bending and finally C-C stretching in phenol ring, respectively. In this system, the diazonium ion are not stable and can change to the para-mercaptophenol form which, can be detected by the SERS measurement. So, para-mercaptophenol are the same function as the capping agent species. The C-C stretching in phenol ring of the capping agent and the analyte are appeared as shown in the same wavenumber at 1571 cm^{-1} . The table of the peak assignment was shown in Table 4.1. These observations confirm the chemical adsorption and the formation of the carbofuran-derived azo compound molecules on the AgNPs surface. From SERS technique, the efficiency of adsorption in a high near electric field is critically affects to the sensitivity of the SERS signal. Therefore, amount of capping agent and analyte diffused close to AgNPs surface is directly proportion to the SERS intensity. 0.1 ppm to 100 ppm. However, only peak of C-C stretching in phenol ring (1570 cm^{-1}) display the characteristic peaks of the analyte derivatives from the capping agent.

Due to the high similarity of chemical structures between *p*-ATP and carbofuran, the intensity of those assigned peaks was increased when the amount of carbofuran was increased from 0.1 – 100 ppm.

Firstly, the number of added capping agent spectra was optimized in order to obtain the best calibration model (R^2 value). The R^2 value of the calibration model at the different sample insertion ratio is shown in Figure 4.5. It can be seen that the R^2 value was reached to 0.99 when the sample ratio at 100 times was used as the constraint in MCR-ALS calculation. Therefore, in the real sample part, the ratio of added capping agent was used at 100 times for extracted the capping agent spectra

Table 4.1 SERS peak assignment for *p*-mercaptophenol and carbofuran-derived azo compound

Raman shift/cm ⁻¹		SERS assignment
para-mercaptophenol	Carbofuran-derived azo compound	
1075	1075	C-S stretching
	1201	C-N stretching, CCN (phenyl-N) in-plane bending, C-H and O-H bending, C-C stretching from phenol group
1327	1333	CCH bending NCC bending with phenyl ring
	1410	-N=N- stretching
1429		C-H and O-H bending from phenol group
1571	1571	C-C stretching within phenol

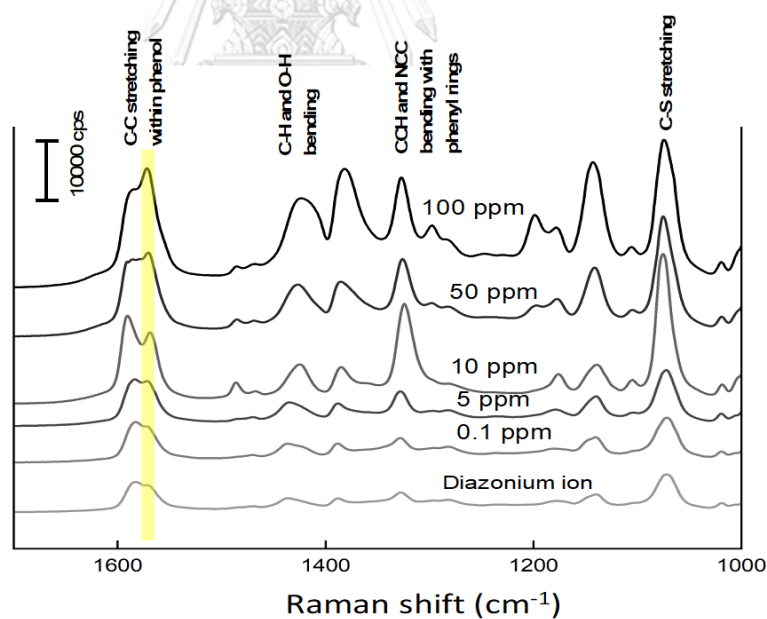


Figure 4.4 SERS spectra of azo compounds derived from carbofuran of 0.1-100 ppm. The yellow highlight is the region that was used to examine the relationship between the intensity and concentration. The yellow highlight is the selected peaks to quantify the amount of cabofuran

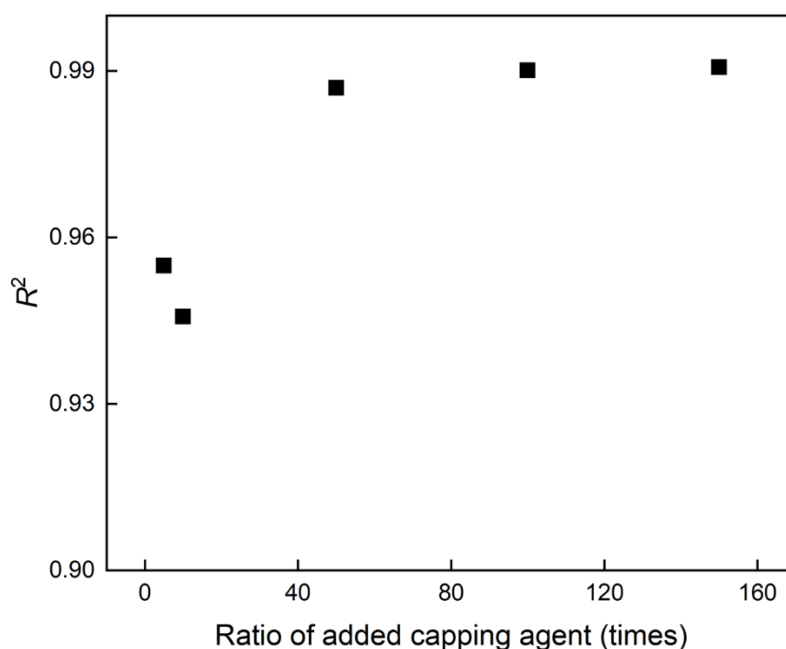


Figure 4.5 The R^2 values of the calibration model using sample insertion constraint with the added capping agent at ratio of 5, 10, 50, 100, and 150 times

To examine the relationship between concentration and intensity of SERS signal, only intensity from the peak at 1570 cm^{-1} (yellow highlight) was used. From Figure 4.6A, the calibration plot using the intensity against the concentration of carbofuran was directly performed from the original SERS spectra (Figure 4.4) The plot can be fitted by linear equation of $A_{1057} = 42.6 C + 5702.6$ where C is the concentration of carbofuran in ppm unit with $R^2 = 0.731$. The limit of detection (LOD) can be calculated as 125.19 ppm. Due to the high overlapping peak, the correlation coefficient (R^2) calculated directly from the peak intensity is not satisfied. In the case, the SERS spectra was projected to our propose method in order to extract the signal from capping agent to remain only the analyte signal. Figure 4.6B shows the extracted SERS spectra of the analyte. The calibration curve elucidated from peak at 1570 cm^{-1} against the carbofuran concentration give a promising R^2 up to 0.99 with the linear equation of $A_{1057} = 28.3 C + 245.3$. The limit of detection (LOD) can be calculated as 28.19 ppm.

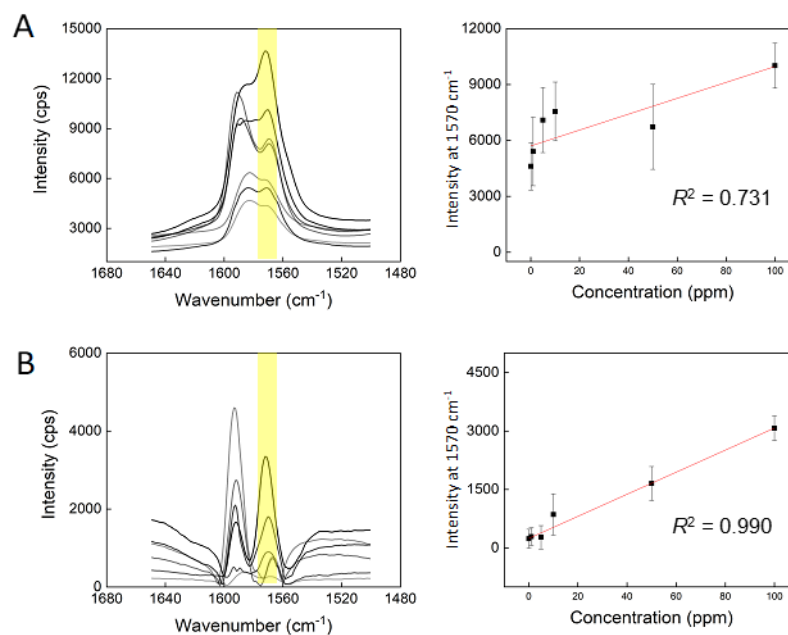


Figure 4.6 (A) SERS spectra of azo compounds at peak 1570 cm⁻¹ and the calibration curve with $R^2 = 0.731$. (B) SERS spectra after MCR-ALS extraction with sample insertion constraint and the calibration curve with $R^2 = 0.990$. The yellow highlight is the peaks corresponding to amount of carbofuran

The concentration of the carbofuran in the calibration and validation set was predicted by the intensity of the extracted spectra and it was shown in Figure 4.7. The relationship between the predicted concentration and the presetting concentration were shown. From the results, the high R^2 values of predicted concentration were obtained in both of calibration ($R^2 = 0.98$) and validation sets ($R^2 = 0.97$). The error of the prediction in the both sets were reported by using root-mean-square error ($RMSE$) value. From the results, the $RMSE = 0.188$ and 2.109 were obtained from calibration and validation set, respectively. The error of the concentration is in the acceptable range. It can be seen that the developed algorithm can eliminate capping agent peak and can be used to quantify the concentration of analyte with high precision and accuracy.

From the results, it shows that the MCR-ALS with sample insertion constraint can be used to exclude the interrupted signal from capping agent in SERS detection

system. This generates the higher correlation coefficient and sensitivity of SERS techniques without any requirement of additional experiments.

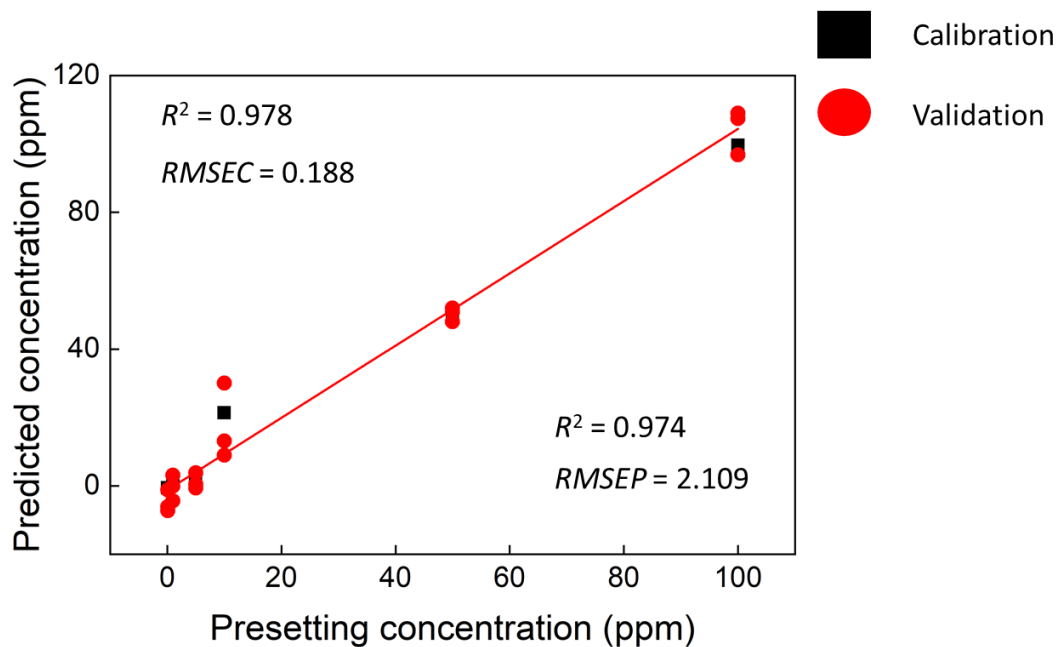


Figure 4.7 Predicted concentration versus presetting concentration in the carbofuran derived azo-compound at the 1570 cm^{-1} peaks the black square and red circle represent the calibration and validation set, respectively by the *RMSEC* is the *RMSE* values of calibration and *RMSEP* is the *RMSE* of the validation sets.

CHAPTER V

CONCLUSION

The MCR-ALS method was successfully modified with sample insertion constraint in order to extract the analyte signal which represents as minor component in SERS measurement. The developed program was elucidated with the simulated spectral data. The simulated spectral data was generated using gaussian distribution function with different overlapping level ($RS = 0$ (completely overlapped) – 1.5 (completely separated)) and different concentration ratios between intensity of capping agent and analyte in the range of 0.01 – 1.00. By using MCR-ALS with sample insertion constraint, the calibration model of the analyte peak in the all conditions, including highly-low overlapping levels, can be generated with high precision ($R^2 > 0.95$) and high accuracy with $MAPE < 20$. Moreover, the influences of the number of spectra which had been added in the calculation were monitored and investigated. The suitable added spectra need to be carefully considered in order to completely exclude the unwanted signals which is capping agent spectra in the case. The appropriate number of added spectra was automatically optimized by using the change of $MAPE$ which less than 5%. Interestingly, it was found that the smaller number of added spectra is required in the system with high concentration ratio, while the large number of added spectra is needed for the condition with low concentration ratio.

In the part of the real experiment on SERS measurement, the carbofuran (analyte) derived azo-coupling with *p*-ATP (capping agent) acquisition was used to validate the developed algorithms. The peaks of the carbofuran overlapped with the azo-compound at 1570 cm^{-1} (The C-C stretching within phenol) was monitored. By using conventional background subtraction technique, the calibration model of the carbofuran was obtained with unsatisfied results of $R^2 = 0.73$ and $LOD = 125.19\text{ ppm}$. The R^2 value of the model were raised to 0.99 and LOD was down to 28.19 ppm when the modified MCR-ALS with sample insertion constraint was used. To inspect the prediction performance, the validation set of spectra were used and the concentrations of carbofuran of the validation set were quantified by the calibration model built from our developed program. It was found that the R^2 value of validation set equal to 0.97 and $RMSE$ with only 2.109 was satisfactory obtained.

APPENDIX

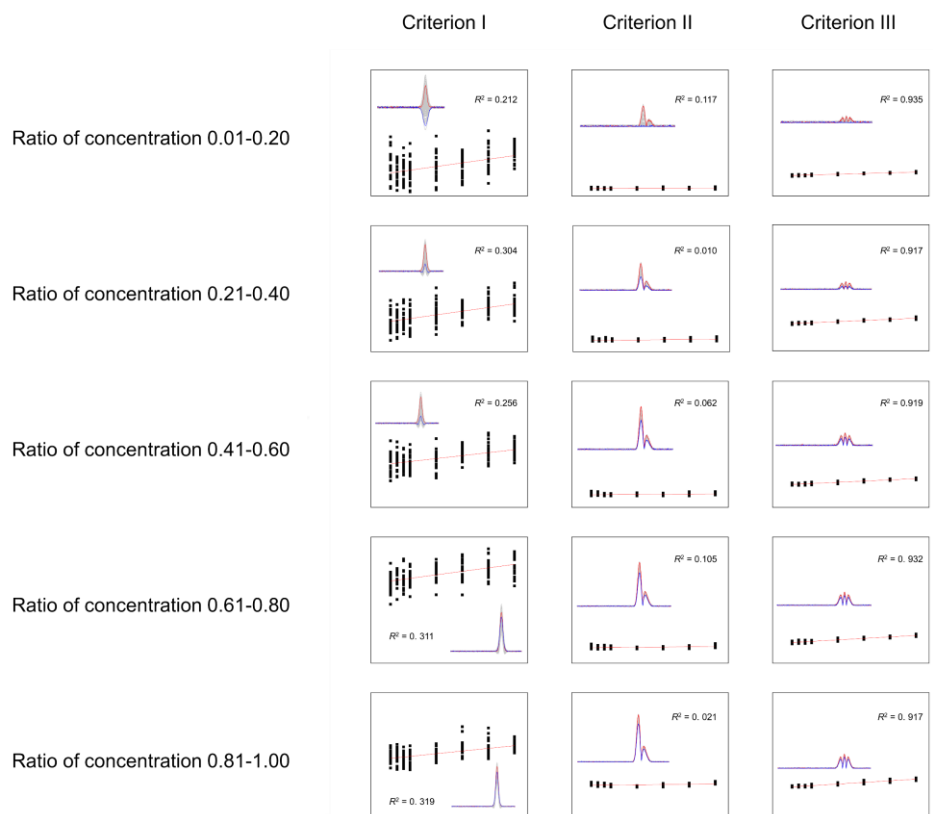


Figure 1 the calibration curve plot from analyte peak extracted by criterion (I) background subtraction, (II) MCR-ALS and (III) MCR-ALS with sample insertion constrain on the $RS = 0$ at the various concentration ratio of the analyte

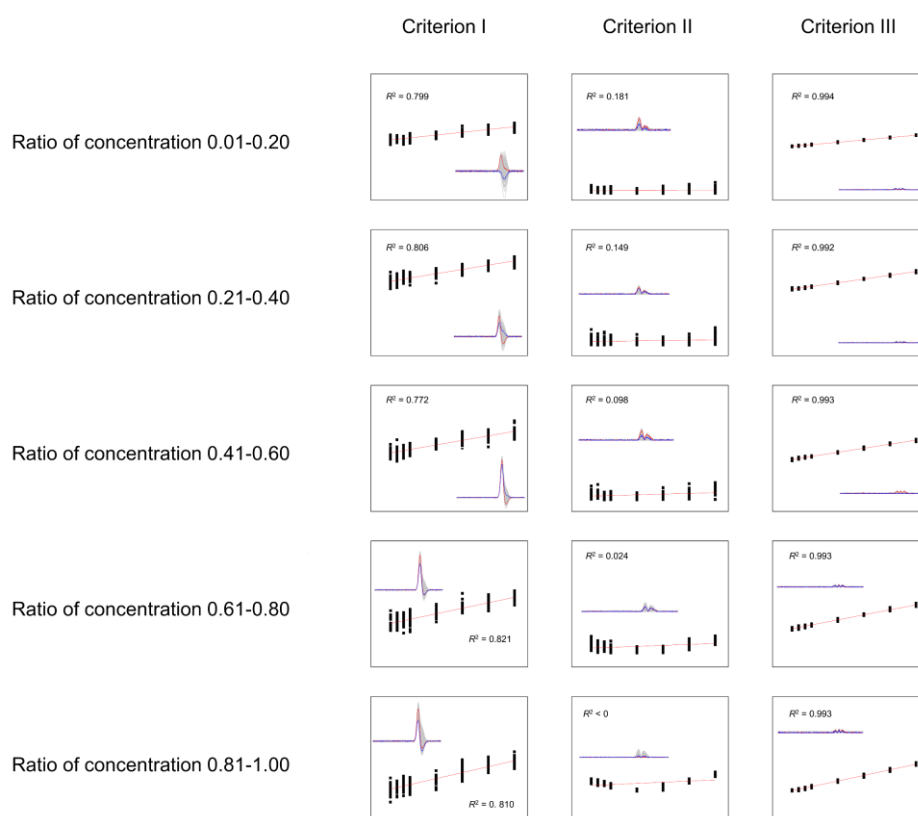


Figure 2 the calibration curve plot from analyte peak extracted by criterion (I) background subtraction, (II) MCR-ALS and (III) MCR-ALS with sample insertion constrain on the $RS = 0.2$ at the various concentration ratio of the analyte

REFERENCES

1. Cottat, M.; D'Andrea, C.; Yasukuni, R.; Malashikhina, N.; Grinyte, R.; Lidgi-Guigui, N.; Fazio, B.; Sutton, A.; Oudar, O.; Charnaux, N.; Pavlov, V.; Toma, A.; Di Fabrizio, E.; Gucciardi, P. G.; Lamy de la Chapelle, M., High Sensitivity, High Selectivity SERS Detection of MnSOD Using Optical Nanoantennas Functionalized with Aptamers. *The Journal of Physical Chemistry C* **2015**, *119* (27), 15532-15540.
2. McNay, G.; Eustace, D.; Smith, W. E.; Faulds, K.; Graham, D., Surface-Enhanced Raman Scattering (SERS) and Surface-Enhanced Resonance Raman Scattering (SERRS): A Review of Applications. *Appl. Spectrosc.* **2011**, *65* (8), 825-837.
3. Senapati, T.; Senapati, D.; Singh, A. K.; Fan, Z.; Kanchanapally, R.; Ray, P. C., Highly selective SERS probe for Hg(II) detection using tryptophan-protected popcorn shaped gold nanoparticles. *Chemical Communications* **2011**, *47* (37), 10326-10328.
4. Wang, Y.; Wei, H.; Li, B.; Ren, W.; Guo, S.; Dong, S.; Wang, E., SERS opens a new way in aptasensor for protein recognition with high sensitivity and selectivity. *Chemical Communications* **2007**, (48), 5220-5222.
5. Cañamares, M. V.; Garcia-Ramos, J. V.; Gómez-Varga, J. D.; Domingo, C.; Sanchez-Cortes, S., Comparative Study of the Morphology, Aggregation, Adherence to Glass, and Surface-Enhanced Raman Scattering Activity of Silver Nanoparticles Prepared by Chemical Reduction of Ag⁺ Using Citrate and Hydroxylamine. *Langmuir* **2005**, *21* (18), 8546-8553.
6. Cui, Q.; Shen, G.; Yan, X.; Li, L.; Möhwald, H.; Bargheer, M., Fabrication of Au@Pt Multibranching Nanoparticles and Their Application to In Situ SERS Monitoring. *ACS Applied Materials & Interfaces* **2014**, *6* (19), 17075-17081.
7. Darienzo, R. E.; Chen, O.; Sullivan, M.; Mironava, T.; Tannenbaum, R., Au nanoparticles for SERS: Temperature-controlled nanoparticle morphologies and their Raman enhancing properties. *Materials Chemistry and Physics* **2020**, *240*, 122143.
8. Lee, C.; Zhang*, P., Facile synthesis of gelatin-protected silver nanoparticles for SERS applications. *Journal of Raman Spectroscopy* **2013**, *44* (6), 823-826.
9. Photopoulos, P.; Boukos, N.; Panagopoulou, M.; Meintanis, N.; Pantiskos, N.; Raptis, Y.; Tsoukalas, D., Size control of Ag nanoparticles for SERS sensing applications. *Procedia Engineering* **2011**, *25*, 280-283.
10. Tian, F.; Bonnier, F.; Casey, A.; Shanahan, A. E.; Byrne, H. J., Surface enhanced Raman scattering with gold nanoparticles: effect of particle shape. *Analytical Methods* **2014**, *6* (22), 9116-9123.
11. Bu, Y.; Lee, S., Influence of Dopamine Concentration and Surface Coverage of Au Shell on the Optical Properties of Au, Ag, and AgcoreAushell Nanoparticles. *ACS Applied Materials & Interfaces* **2012**, *4* (8), 3923-3931.
12. Liu, P.; Yang, S.; Fang, M.; Luo, X.; Cai, W., Complex nanostructures synthesized from nanoparticle colloids under an external electric field. *Nanoscale* **2011**, *3* (9), 3933-3940.
13. Song, W.; Ji, W.; Vantasin, S.; Tanabe, I.; Zhao, B.; Ozaki, Y., Fabrication of a highly sensitive surface-enhanced Raman scattering substrate for monitoring the catalytic degradation of organic pollutants. *Journal of Materials Chemistry A* **2015**, *3* (25), 13556-13562.
14. Sun, F.; Galvan, D. D.; Jain, P.; Yu, Q., Multi-functional, thiophenol-based

surface chemistry for surface-enhanced Raman spectroscopy. *Chemical Communications* **2017**, 53 (33), 4550-4561.

15. Kamińska, A.; Witkowska, E.; Winkler, K.; Dzięcielewski, I.; Weyher, J.; Waluk, J., Detection of Hepatitis B virus antigen from human blood: SERS immunoassay in a microfluidic system. *Biosensors & bioelectronics* **2014**, 66C, 461-467.

16. Lee, H.; Liao, J.-D.; Sivashanmugan, K.; Liu, B.; Fu, W.-E.; Chen, C.-C.; Chen, G.; Juang, Y., Gold Nanoparticle-Coated ZrO₂-Nanofiber Surface as a SERS-Active Substrate for Trace Detection of Pesticide Residue. *Nanomaterials* **2018**, 8, 402.

17. Nima, Z. A.; Mahmood, M.; Xu, Y.; Mustafa, T.; Watanabe, F.; Nedosekin, D. A.; Juratli, M. A.; Fahmi, T.; Galanzha, E. I.; Nolan, J. P.; Basnakian, A. G.; Zharov, V. P.; Biris, A. S., Circulating tumor cell identification by functionalized silver-gold nanorods with multicolor, super-enhanced SERS and photothermal resonances. *Scientific Reports* **2014**, 4 (1), 4752.

18. Song, W.; Nie, G.; Ji, W.; Jiang, Y.; Lu, X.; Zhao, B.; Ozaki, Y., Synthesis of bifunctional reduced graphene oxide/CuS/Au composite nanosheets for in situ monitoring of a peroxidase-like catalytic reaction by surface-enhanced Raman spectroscopy. *RSC Advances* **2016**, 6 (59), 54456-54462.

19. Sun, F.; Bai, T.; Zhang, L.; Ella-Menye, J.-R.; Liu, S.; Nowinski, A. K.; Jiang, S.; Yu, Q., Sensitive and Fast Detection of Fructose in Complex Media via Symmetry Breaking and Signal Amplification Using Surface-Enhanced Raman Spectroscopy. *Analytical Chemistry* **2014**, 86 (5), 2387-2394.

20. Sivanesan, A.; Witkowska, E.; Adamkiewicz, W.; Dziewit, Ł.; Kamińska, A.; Waluk, J., Nanostructured silver-gold bimetallic SERS substrates for selective identification of bacteria in human blood. *Analyst* **2014**, 139 (5), 1037-1043.

21. Ye, Y.; Liu, H.; Yang, L.; Liu, J., Sensitive and selective SERS probe for trivalent chromium detection using citrate attached gold nanoparticles. *Nanoscale* **2012**, 4 (20), 6442-6448.

22. Meksiarun, P.; Ishigaki, M.; Huck-Pezzei, V. A. C.; Huck, C. W.; Wongravee, K.; Sato, H.; Ozaki, Y., Comparison of multivariate analysis methods for extracting the paraffin component from the paraffin-embedded cancer tissue spectra for Raman imaging. *Scientific Reports* **2017**, 7 (1), 44890.

23. Villa, J. E. L.; Poppi, R. J., A portable SERS method for the determination of uric acid using a paper-based substrate and multivariate curve resolution. *Analyst* **2016**, 141 (6), 1966-1972.

24. Vrabie, V.; Gobinet, C.; Piot, O.; Tfayli, A.; Bernard, P.; Huez, R.; Manfait, M., Independent component analysis of Raman spectra: Application on paraffin-embedded skin biopsies. *Biomedical Signal Processing and Control* **2007**, 2 (1), 40-50.

25. Yu, Z.; Grasso, M. F.; Sorensen, H. H.; Zhang, P., Ratiometric SERS detection of polycyclic aromatic hydrocarbons assisted by β -cyclodextrin-modified gold nanoparticles. *Microchimica Acta* **2019**, 186 (6), 391.

26. Bernuy, B.; Meurens, M.; Mignolet, E.; Larondelle, Y., Performance Comparison of UV and FT-Raman Spectroscopy in the Determination of Conjugated Linoleic Acids in Cow Milk Fat. *Journal of Agricultural and Food Chemistry* **2008**, 56 (4), 1159-1163.

27. Lai, K.; Zhang, Y.; Du, R.; Zhai, F.; Rasco, B. A.; Huang, Y., Determination of chloramphenicol and crystal violet with surface enhanced Raman spectroscopy. *Sensing*

and Instrumentation for Food Quality and Safety **2011**, 5 (1), 19-24.

28. Lee, K.-M.; Herrman, T. J.; Bisrat, Y.; Murray, S. C., Feasibility of Surface-Enhanced Raman Spectroscopy for Rapid Detection of Aflatoxins in Maize. *Journal of Agricultural and Food Chemistry* **2014**, 62 (19), 4466-4474.
29. Seasholtz, M. B.; Archibald, D. D.; Lorber, A.; Kowalski, B. R., Quantitative Analysis of Liquid Fuel Mixtures with the Use of Fourier Transform Near-IR Raman Spectroscopy. *Appl. Spectrosc.* **1989**, 43 (6), 1067-1072.
30. Cooper, J. B., Chemometric analysis of Raman spectroscopic data for process control applications. *Chemometrics and Intelligent Laboratory Systems* **1999**, 46 (2), 231-247.
31. Penido, C. A. F. d. O.; Silveira, L.; Pacheco, M. T. T., Quantification of binary mixtures of cocaine and adulterants using dispersive Raman and FT-IR spectroscopy and principal component regression. *Instrumentation Science & Technology* **2012**, 40 (5), 441-456.
32. Sivakesava, S.; Irudayaraj, J.; Ali, D., Simultaneous determination of multiple components in lactic acid fermentation using FT-MIR, NIR, and FT-Raman spectroscopic techniques. *Process Biochemistry* **2001**, 37 (4), 371-378.
33. Ashton, L.; Brewster, V. L.; Correa, E.; Goodacre, R., Detection of glycosylation and iron-binding protein modifications using Raman spectroscopy. *Analyst* **2017**, 142 (5), 808-814.
34. Lemoine, É.; Dallaire, F.; Yadav, R.; Agarwal, R.; Kadoury, S.; Trudel, D.; Guiot, M.-C.; Petrecca, K.; Leblond, F., Feature engineering applied to intraoperative in vivo Raman spectroscopy sheds light on molecular processes in brain cancer: a retrospective study of 65 patients. *Analyst* **2019**, 144 (22), 6517-6532.
35. Czaja, T.; Wójcik, K.; Grzeszczuk, M.; Szostak, R., Polypyrrole-Methyl Orange Raman pH Sensor. *Polymers (Basel)* **2019**, 11 (4), 715.
36. Zhao, X.; He, Y.; Liu, Z.; Zhang, W.; Tong, L., Method for extracting Raman spectra characteristic variables of biological sample based on Hilbert-Huang transform. *Journal of Raman Spectroscopy* **2020**, 51 (6), 1019-1028.
37. Krause, S.; Overgaard, M. H.; Vosch, T., Photon Energy Dependent Micro-Raman Spectroscopy with a Continuum Laser Source. *Scientific Reports* **2018**, 8 (1), 11621.
38. Gautam, R.; Vanga, S.; Ariese, F.; Umaphathy, S., Review of multidimensional data processing approaches for Raman and infrared spectroscopy. *EPJ Techniques and Instrumentation* **2015**, 2 (1), 8.
39. Van de Sompel, D.; Garai, E.; Zavaleta, C.; Gambhir, S. S., A hybrid least squares and principal component analysis algorithm for Raman spectroscopy. *PLoS One* **2012**, 7 (6), e38850-e38850.
40. Miller, C.E. Chemometrics in Process Analytical Technology (PAT). *Process Analytical Technology*, pp 353-438.
41. Hancewicz, T. M.; Petty, C., Quantitative analysis of vitamin A using Fourier transform Raman spectroscopy. *Spectrochimica Acta Part A: Molecular and Biomolecular Spectroscopy* **1995**, 51 (12), 2193-2198.
42. Kachrimanis, K.; Braun, D. E.; Griesser, U. J., Quantitative analysis of paracetamol polymorphs in powder mixtures by FT-Raman spectroscopy and PLS regression. *Journal of Pharmaceutical and Biomedical Analysis* **2007**, 43 (2), 407-412.
43. Li, S.; Gao, J.; Nyagilo, J. O.; Dave, D. P. Probabilistic Partial Least Square

Regression: A Robust Model for Quantitative Analysis of Raman Spectroscopy Data, 2011 *IEEE International Conference on Bioinformatics and Biomedicine*, 12-15 Nov. 2011; 2011; pp 526-531.

44. Zhang, L.; Li, Q.; Tao, W.; Yu, B.; Du, Y., Quantitative analysis of thymine with surface-enhanced Raman spectroscopy and partial least squares (PLS) regression. *Analytical and Bioanalytical Chemistry* **2010**, *398* (4), 1827-1832.

45. Oleneva, E.; Khaydukova, M.; Ashina, J.; Yaroshenko, I.; Jahatspanian, I.; Legin, A.; Kirsanov, D., A Simple Procedure to Assess Limit of Detection for Multisensor Systems. *Sensors (Basel)* **2019**, *19* (6), 1359.

46. Bayat, M.; Marín-García, M.; Ghasemi, J. B.; Tauler, R., Application of the area correlation constraint in the MCR-ALS quantitative analysis of complex mixture samples. *Analytica Chimica Acta* **2020**, *1113*, 52-65.

47. Bertinetto, C. G.; de Juan, A., Systematic comparison and potential combination between multivariate curve resolution–alternating least squares (MCR-ALS) and band-target entropy minimization (BTEM). *Journal of Chemometrics* **2018**, *32* (6), e3000.

48. Mamián-López, M. B.; Poppi, R. J., SERS hyperspectral imaging assisted by MCR-ALS for studying polymeric microfilms loaded with paracetamol. *Microchemical Journal* **2015**, *123*, 243-251.

49. Smith, J. P.; Holahan, E. C.; Smith, F. C.; Marrero, V.; Booksh, K. S., A novel multivariate curve resolution-alternating least squares (MCR-ALS) methodology for application in hyperspectral Raman imaging analysis. *Analyst* **2019**, *144* (18), 5425-5438.

50. Villa, J. E. L.; Afonso, M. A. S.; dos Santos, D. P.; Mercadal, P. A.; Coronado, E. A.; Poppi, R. J., Colloidal gold clusters formation and chemometrics for direct SERS determination of bioanalytes in complex media. *Spectrochimica Acta Part A: Molecular and Biomolecular Spectroscopy* **2020**, *224*, 117380.

51. Villa, J. E. L.; Pasquini, C.; Poppi, R. J., Surface-enhanced Raman spectroscopy and MCR-ALS for the selective sensing of urinary adenosine on filter paper. *Talanta* **2018**, *187*, 99-105.

52. Vosough, M.; Mashhadiabbas Esfahani, H., Fast HPLC-DAD quantification procedure for selected sulfonamids, metronidazole and chloramphenicol in wastewaters using second-order calibration based on MCR-ALS. *Talanta* **2013**, *113*, 68-75.

53. Pérez, R. L.; Escandar, G. M., Liquid chromatography with diode array detection and multivariate curve resolution for the selective and sensitive quantification of estrogens in natural waters. *Analytica Chimica Acta* **2014**, *835*, 19-28.

54. Wang, Y.; Hu, J.; Zhuang, Q.; Ni, Y., Enhancing sensitivity and selectivity in a label-free colorimetric sensor for detection of iron(II) ions with luminescent molybdenum disulfide nanosheet-based peroxidase mimetics. *Biosensors and Bioelectronics* **2016**, *80*, 111-117.

55. Sukmanee, T.; Wongravee, K.; Ekgasit, S.; Thammacharoen, C.; Pienpinijtham, P., Facile and Sensitive Detection of Carbofuran Carbamate Pesticide in Rice and Soybean Using Coupling Reaction-based Surface-Enhanced Raman Scattering. *Analytical Sciences* **2017**, *33* (1), 89-94.

56. Smith, E.; Dent, G., Modern Raman spectroscopy: a practical approach. *John Wiley & Sons Ltd: Chichester, UK*, **2005**.

57. Larkin, P., Infrared and Raman spectroscopy: principles and spectral interpretation. *Elsevier*: **2017**.

58. Abalde-Cela, S.; Aldeanueva-Potel, P.; Mateo-Mateo, C.; Rodríguez-Lorenzo, L.; Alvarez-Puebla, R. A.; Liz-Marzán, L. M., Surface-enhanced Raman scattering biomedical applications of plasmonic colloidal particles. *Journal of The Royal Society Interface* **2010**, *7* (suppl_4), S435-S450.
59. Pilot, R.; Signorini, R.; Durante, C.; Orian, L.; Bhamidipati, M.; Fabris, L., A Review on Surface-Enhanced Raman Scattering. *Biosensors (Basel)* **2019**, *9* (2), 57.
60. Petryayeva, E.; Krull, U. J., Localized surface plasmon resonance: Nanostructures, bioassays and biosensing—A review. *Analytica Chimica Acta* **2011**, *706* (1), 8-24.
61. Botta, R.; Chindaudom, P.; Eiamchai, P.; Horprathum, M.; Limwichean, S.; Chananonawathorn, C.; Patthanasettakul, V.; Kaewseekhao, B.; Faksri, K.; Nuntawong, N., Tuberculosis determination using SERS and chemometric methods. *Tuberculosis* **2018**, *108*, 195-200.
62. Zhu, J.; Agyekum, A. A.; Kutsanedzie, F. Y. H.; Li, H.; Chen, Q.; Ouyang, Q.; Jiang, H., Qualitative and quantitative analysis of chlorpyrifos residues in tea by surface-enhanced Raman spectroscopy (SERS) combined with chemometric models. *LWT* **2018**, *97*, 760-769.
63. Xu, J.; Du, J.; Jing, C.; Zhang, Y.; Cui, J., Facile Detection of Polycyclic Aromatic Hydrocarbons by a Surface-Enhanced Raman Scattering Sensor Based on the Au Coffee Ring Effect. *ACS Applied Materials & Interfaces* **2014**, *6* (9), 6891-6897.
64. Vongsvivut, J.; Robertson, E. G.; McNaughton, D., Surface-enhanced Raman spectroscopic analysis of fonofos pesticide adsorbed on silver and gold nanoparticles. *Journal of Raman Spectroscopy* **2010**, *41* (10), 1137-1148.
65. Kulthe, A. A.; Pawar, V. D.; Kotecha, P. M.; Chavan, U. D.; Bansode, V. V., Development of high protein and low calorie cookies. *J Food Sci Technol* **2014**, *51* (1), 153-157.
66. De Juan, A.; Tauler, R., Multivariate curve resolution-alternating least squares for spectroscopic data. *Data Handling in Science and Technology*, Elsevier: **2016**; Vol. 30, pp 5-51.
67. Chen, J.; Richard, C.; Bermudez, J. C. M.; Honeine, P., Nonnegative least-mean-square algorithm. *IEEE Transactions on Signal Processing* **2011**, *59* (11), 5225-5235.
68. Jaumot, J.; de Juan, A.; Tauler, R., MCR-ALS GUI 2.0: New features and applications. *Chemometrics and Intelligent Laboratory Systems* **2015**, *140*, 1-12.
69. Ozek, M. B.; Akpolat, Z. H., A software tool: Type-2 fuzzy logic toolbox. *Computer Applications in Engineering Education* **2008**, *16* (2), 137-146.
70. Lee, P.; Meisel, D., Adsorption and surface-enhanced Raman of dyes on silver and gold sols. *The Journal of Physical Chemistry* **1982**, *86* (17), 3391-3395.

VITA

NAME	Nontawat Sricharoen
DATE OF BIRTH	21 Feb 1995
PLACE OF BIRTH	Nakorn Si Thammarat
HOME ADDRESS	6 M.5 T.Chain Yai A.Chaiyai Nakorn Si Thammarat

